Omics-based insights into human liver reveal GTPase-driven mechanisms of MASLD progression in obesity

Qing Zhao[1,2,3*], William De Nardo[4*], Ruoyu Wang[5,10*], Yi Zhong[8], Umur Keles[10], Li Na Zhao[10], Huiyi Tay[1,2], Sonia Youhanna[8], Mengchao Yan[9], Ye Xie[9], Youngrae Kim[1,2], Sungdong Lee[1,2], Rachel Liyu Lim[1,2], Guoshou Teo[1,2], Pradeep Narayanaswamy[7], Paul R. Burton[6], Volker M. Lauschke[8,9], Hyungwon Choi[1,2,3#], Matthew J. Watt[4,#], and Philipp Kaldis[10,#,&]

[1]Department of Medicine, Yong Loo Lin School of Medicine, National University of Singapore, Singapore
[2]Singapore Lipidomics Incubator, Life Sciences Institute, National University of Singapore, Singapore
[3]Cardiovascular & Metabolic Disease Translational Research Programme, Yong Loo Lin School of Medicine, National University of Singapore, Singapore
[4]Department of Anatomy and Physiology, School of Biomedical Sciences, Faculty of Medicine Dentistry and Health Sciences, University of Melbourne, Melbourne, Victoria, Australia
[5]Department of Hepatology, The First Hospital of Hunan University of Chinese Medicine, Changsha, Hunan, China
[6]Department of Surgery, School of Translational Medicine, Monash University, Melbourne, Victoria, 3004, Australia and Bariatric Unit, Department of General Surgery, The Alfred Hospital, Melbourne, Victoria, 3004, Australia
[7]SCIEX, R&D, Singapore
[8]Department of Physiology and Pharmacology and Centre of Molecular Medicine, Karolinska Institutet, 171 77 Stockholm, Sweden
[9]Dr. Margarete Fischer-Bosch Institute of Clinical Pharmacology, Stuttgart, Germany.
[10]Department of Clinical Sciences Malmö, Lund University, Clinical Research Centre (CRC), Sweden

[#]Correspondence should be addressed to PK (phone +4673 776 8101; philipp.kaldis@med.lu.se), MJW (matt.watt@unimelb.edu.au) or HC (hyung_won_choi@nus.edu.sg) – [&]Lead Contact

Running title: GTPase signaling underlies MASLD progression

Keywords: Metabolic dysfunction-associated steatotic liver disease; Lipid metabolism; Liver fibrosis; GTPase signaling

Abstract

Metabolic dysfunction-associated steatotic liver disease (MASLD) is generally asymptomatic in the early stages but, without appropriate intervention, it can progress to severe liver morbidities. To elucidate the molecular mechanisms of early development of MASLD, we performed transcriptomic analysis on liver biopsies and metabolomic analysis on liver and plasma samples from 109 obese individuals with no liver pathology or early stages of MASLD. The liver metabolome is remodeled by the parenchymal accumulation of neutral lipids, whereas the plasma metabolome displayed little differences. The liver transcriptome revealed that the progression of steatosis and fibrosis is characterized by distinct gene expression signatures. While metabolic remodeling characterizes steatosis, global rewiring of gene expression underpins fibrosis progression. Importantly, GTPases and their regulators were identified as a novel signature for the transition from steatosis to fibrosis. GTPase genes and their regulators were associated with hepatic fibrosis grades and co-expressed with TGF-β signaling. We further verified the involvement of GTPase regulation in fibrogenesis in HSC-like LX-2 cells and a 3D liver spheroid model of primary human hepatocytes and non-parenchymal cells. Our study suggests that modulation of GTPase signaling is a potential therapeutic entry point for the treatment of early liver fibrosis in MASLD.

Highlights

- Liver metabolome remodeling is marked by accumulation of neutral lipids and relative reduction of glycerophospholipids and sphingolipids. Changes in the plasma metabolome were poorly correlated with the changes in the liver metabolome in early-stage MASLD.

- Steatosis is closely linked to metabolic remodeling, whereas fibrosis progression is associated with global rewiring of gene expression.
- Over 200 genes were identified as progressive markers for fibrosis progression.
- GTPase signaling emerged as the top enriched pathway involved in the transition from non-fibrotic steatosis to the onset of fibrosis. The involvement of GTPase and its regulation in liver fibrogenesis was validated in a 3D spheroid MASH model. Pharmacological-mediated GTPase inhibition hindered collagen production in HSC-like LX-2 cells.

Introduction

Metabolic dysfunction-associated steatotic liver disease (MASLD) is the most common chronic liver disease, affecting over 30% of adults worldwide (1). The prevalence of MASLD is closely associated with the epidemic of obesity, which has been increasing globally over the years (2). As the liver manifestation of the metabolic syndrome, MASLD can cause and is also affected by concurrent metabolic abnormalities commonly seen in obese individuals, such as insulin resistance, diabetes, dyslipidemia , and hypertension (3, 4). Early stages of MASLD are characterized by hepatic steatosis, which is the excessive deposition of triacylglycerol (TAG) rich lipid droplets within the liver parenchyma and is usually reversible. However, in a subset of patients, the disease can develop into inflammatory and ballooning stages termed metabolic dysfunction-associated steatohepatitis (MASH), a more severe form of the disease with an increased incidence and severity of fibrosis. The primary risk of hepatic fibrosis is its potential to progress to cirrhosis, for which there are currently no effective treatments, and to hepatocellular carcinoma, a lethal malignancy (5, 6).

Metabolic dysfunction is a primary feature and contributor of MASLD pathogenesis (7). Hepatic steatosis is often accompanied by abnormal gluconeogenesis and dysregulated glucose metabolism (8) as well as disrupted cholesterol homeostasis which becomes apparent with MASLD progression (9). Mitochondria, as the main hubs of cellular energy metabolism, are affected by the metabolic abnormality in liver diseases (10). These interconnected metabolic phenotypes form the basis for the development of MASLD (11, 12). Recent advancements in metabolomics and lipidomics have greatly enhanced the understanding of the molecular systems biology of MASLD (13, 14), however, few

studies have combined such analysis with transcriptomics to provide integrative insights into disease pathogenesis in humans.

Fibrosis is the only histological feature of MASLD that correlates with liver-related mortality and morbidity (15). In the injured liver, damaged and dead hepatocytes modulate the crosstalk between hepatocytes, liver macrophages, and hepatic stellate cells (HSCs) by releasing fibrogenic cytokines (e.g., TGF-β1) and activating multiple signaling pathways (16, 17). As a result of the multicellular response, HSCs transdifferentiate into active, collagen-producing myofibroblasts, driving fibrogenesis and the excessive deposition of extracellular matrix (ECM) (17). Since fibrosis is a key prognostic marker of MASLD progression, the shift from simple steatosis to fibrosis marks a critical point in the disease, offering a key opportunity for intervention to prevent further progression (18). Despite the availability of certain guidelines for clinical management of MASLD (19), the molecular and metabolic changes underpinning the key transitions driving disease progression in the context of obesity remain poorly understood. This poses a challenge to early disease management and prevention.

In this study, we generated a comprehensive map of gene expression and metabolomic profiles to delineate the molecular events driving early-stage MASLD progression in obese patients. This multi-omic resource focused our investigation on key molecular changes associated with (a) the transition from obesity without hepatic pathology to MASLD and (b) the onset of liver fibrosis. Our results indicate that changes in metabolism underpin the development of steatosis exclusively, while gene expression alterations in the liver are closely linked to fibrosis, highlighting the distinct molecular drivers across MASLD stages. Notably, the expression of numerous GTPases and their regulators were identified as a new signature that marks the onset of liver fibrosis, which has not been widely investigated in the context of liver fibrosis.

The involvement of GTPase signaling in fibrosis development was further validated in LX-2 HSCs and a 3D liver spheroid system of human MASH. Overall, this study provides a deep molecular and metabolomic examination of the liver in obese persons with early MASLD and identifies potential therapeutic targets for reversing fibrosis in its early stages.

Results

Overview of the study

This study enrolled 109 obese patients who were considered for bariatric surgery at The Avenue, Cabrini, or Alfred Hospitals in Melbourne, Australia. The cohort consists of 33 individuals without liver pathology, 65 with MASL, and 11 with MASH (Figure 1A). The demographic and clinical characteristics of the cohort are summarized in Table 1. In this cohort, 74 individuals (68%) had grade 0 or 1 steatosis and 83 (76%) had grade 0 or 1 fibrosis. Hepatic inflammation and ballooning were mild and uncommon, with 9 cases exhibiting grade 2 or higher inflammation and only one case showing grade 2 ballooning (Figure 1B). As such, the focus of this study is on the early stages of the MASLD spectrum. In clinical tests, we observed that patients with liver fibrosis exhibited a strong correlation with insulin resistance, while steatosis grades were most correlated with plasma lipids assays (Figure 1D). We performed parallel profiling of the transcriptome in liver slices and the metabolome in the liver, plasma, and conditioned medium (CM, containing secreted factors) from precision-cut liver slices in parallel to construct a comprehensive map of the molecular changes associated with the initiation and progression of MASLD in obese individuals. Moreover, we compared our data with those from two additional cohorts: the Virginia cohort (VA cohort, GSE130970) (20) with a disease spectrum comparable to that of

our study, and the European cohort (EU cohort, GSE135251) (21) with a broader spectrum covering more advanced MASLD pathologies (Figure 1C).

The liver and plasma metabolome of MASLD patients

Using untargeted metabolomics analysis, we identified 1104 metabolites in the liver, 504 in the CM, and 962 in the plasma (Figure 2A). Principal component analysis (PCA) revealed that both glycerolipids (GLs) and non-GL metabolome clustered in the liver progressively from no pathology to MASH (Supplemental figure 1A). Nonetheless, the plasma metabolome did not cluster by MASLD histological analyses. This reflects that metabolic alterations in hepatic tissues were not the dominant contributor to the plasma metabolome at the early stages of MASLD.

Alterations in the plasma metabolome

The plasma metabolome displayed limited changes associated with liver histological features, with statistically significant associations primarily with steatosis, such as TAGs (q value < 0.05, n = 13) and ether-linked TAG (TAG-O, q value < 0.05, n = 5) species. No specific polar metabolite was significantly associated with hepatic histological features. Overall, the plasma metabolome thus poorly mirrored the changes in the liver metabolome in obese individuals with early-stage MASLD.

Remodeling of the liver metabolome

In contrast to the plasma metabolome, the liver metabolome was extensively remodeled in individuals with MASLD. Analysis of the liver metabolome revealed that 637 metabolites (58%), including 453 lipids, showed a significant linear association with histological grades after adjusting for age, gender, adiposity (body mass index, BMI), and diabetes (Figure 2B). As expected, a pronounced change in the hepatic lipidome was the major hallmark of MASLD, reflecting increased storage of GLs and

decreased levels of membrane lipid classes, namely glycerophospholipids (GPLs) and sphingolipids (Figure 2B and 2D). Specifically, TAGs with 0 to 5 double bonds in the fatty acyl chains were positively associated with the histological outcomes, whereas TAGs likely containing at least one polyunsaturated fatty acid (PUFA) chain (number of double bonds> 5) were negatively associated with disease progression, particularly with steatosis (Figure 2C).

Mitochondrial lipids also displayed notable changes in MASLD. The levels of hepatic long-chain acyl-carnitines species decreased in the liver (Supporting data – Supplemental figure 1C), suggesting dysregulated transmembrane transport and β-oxidation of fatty acids in hepatocytes as steatosis advances. We also detected an increase in intermediates of the antioxidant Coenzyme Q10 (CoQ10; ubiquinone), in particular CoQ6 and CoQ9 (Figure 2E), and increased levels of two other antioxidants, taurine and alpha-tocopherol (Vitamin E) in the steatotic liver. Furthermore, the levels of amino acids in the liver were significantly associated with steatosis, including an increase in glutamic acid, arginine, glycine, serine, and alanine (Figure 2E), which are among the major components in collagen and its precursors (22), Thus, ECM regulation may profoundly impact intracellular amino acid dynamics in MASLD patients. In contrast, the aromatic amino acids tryptophan and phenylalanine were decreased in the liver with advancing steatosis. Notably, there was a significant increase in homocysteine and its upstream metabolite S-adenosylhomocysteine, accompanied by a decrease in GNMT mRNA levels (Figure 2E and S3). These changes, along with the elevated levels of the aforementioned collagen-generating metabolites, could be indicative of excessive retinol release following HSC activation (23) or could suggest a feedback loop between HSCs and hepatocytes.

Integrative metabolomic analysis of liver, CM, and plasma

Aligning with the drastic changes in the liver metabolome, metabolites secreted into CM from precision-cut liver slices closely correlated with liver steatosis, particularly mirroring hepatic alterations in GLs and membrane lipid levels (Supplemental figure 1C). In the liver, CM, and plasma, eight common TAG species displayed increasing trends as steatosis progressed (Supplemental figure 2D), reflecting increased secretion of TAG-rich very low-density lipoprotein (VLDL) particles from the liver into the bloodstream. Next, we correlated all molecular features from liver, plasma, and CM using a partial correlation network analysis (24). Metabolites within the same sample matrix displayed correlated patterns; however, inter-matrix connections remained limited (Supplemental figure 1E). Of the 603 metabolites commonly detected in both liver and plasma, only 53 showed a correlation between their respective levels in the liver and plasma (Pearson's $r > 0.5$, Supplemental figure 1B). Therefore, in this cohort, the metabolome of liver and plasma remained largely independent of each other during the early development of MASLD. This underscores the challenges of patient stratification based on plasma metabolite biomarkers in obese individuals with MASLD.

Unique gene expression signatures in hepatic steatosis and fibrosis

To examine the transcriptomic alterations during MASLD progression, bulk RNA sequencing was performed on the liver tissue biopsies. A total of 11,771 expressed genes were analyzed, of which 1,164 (9.9%) were positively and 814 (6.9%) were negatively associated with steatosis or fibrosis (q value < 0.05, Figure 3A). PCA plots indicated that patients with different grades of histological changes were not well clustered along major principal components (Supplemental figure 4). This observation suggests that the liver gene expression profile was not significantly reprogrammed at early-stage MASLD in obese patients. Sparse PCA revealed that potential

confounding factors, such as metabolic processes (first PC) and other biological processes (e.g., translation and ribosome biogenesis, second PC) drive the major transcriptomic variations in early MASLD (Supplemental Table 1). We next identified 992 and 1251 gene markers associated with the histological features of steatosis and fibrosis, respectively (q value < 0.05), adjusting for key clinical variables as in the metabolomic analysis. We observed limited overlapping signatures between steatosis and fibrosis, indicating that unique transcriptomic regulations underlie steatosis and fibrosis, respectively (Figure 3A).

We next performed gene ontology over-representation analysis to unravel biological pathways implicated in the development of MASLD histological features (Supporting data – Figure 3B). Progression of steatosis was characterized by upregulation of pathways related to protein metabolism (25), apoptosis, and the innate immune response (Figure 3B). In line with the extensive remodeling of the liver metabolome, gene signatures associated with the metabolism of carbohydrates, phospholipids, triglycerides, and sphingolipids were significantly downregulated at the expression level.

The development of fibrosis was largely characterized by an upregulation of ECM remodeling, signaling transduction (TLR, NF-kappaB, Wnt), actin cytoskeleton organization, and other well-established fibrosis pathways [e.g., TGF-β signaling] (Figure 3B) (26). Notably, small GTPase-mediated signal transduction is one of the central nodes in the enrichment map of fibrosis-associated genes. In contrast to the upregulation of various metabolic pathways regulated by steatosis, higher fibrosis grades correlated with the downregulation of metabolite processes for xenobiotics, fatty acids, lipids, cellular nitrogen compounds, and bile acids. Downregulated oxidation-reduction process and respiratory electron transport chain were also

identified with higher grade fibrosis, indicative of mitochondrial dysfunction (Figure 3B).

Gene expression signatures underlying metabolic alterations in the liver

To investigate the dysregulation of hepatic lipid metabolism further, we focused on gene alteration patterns in lipid metabolism pathways and compared our observations with those from the EU and VA cohorts (20, 21) (Figure 4A). Consistent with the observations in the liver lipidome, we identified marker genes implicated in the homeostasis of GLs and GPLs (Figure 4B). Genes such as *DGAT2*, *PNPLA3*, and *PLIN3*, which play a role in lipid droplet (LD) formation and TAG and DAG metabolism, displayed significant associations with hepatic histological features (27).

In patients with more advanced hepatic fibrosis, expression levels of genes involved in primary bile acid biosynthesis decreased, such as *AKR1C4*, *ACOX2*, *AMACR*, *SLC27A5*, and *BAAT*. Meanwhile, the expression levels of the primary bile acid mediator, farnesoid X receptor (FXR, encoded by the *NR1H4* gene), also decreased. In addition, a group of cytochrome P450 (CYP) genes were downregulated, implying a reduction in CYP-dependent PUFA metabolism (i.e., linoleic acids and arachidonic acids) and steroid hormone biosynthesis along with the progression of fibrosis (Figure 4A) (28, 29). These alterations highlight metabolic dysfunction that accompanies the development of fibrosis.

To obtain systematic insights into mitochondrial functions beyond β-oxidation, we mapped steatosis and fibrosis marker genes to MitoCarta3.0 (30). Interestingly, disrupted hepatic mitochondrial functions in MASLD patients manifest in various aspects, with distinct patterns for steatosis and fibrosis (Figure 4, C and D). With steatosis progression, 26 mitochondria-related genes were downregulated and 55 genes were upregulated, including 16 involved in the mitochondrial mtDNA

maintenance (Supporting data – Figure 4D). In contrast, fibrosis levels were associated with 151 downregulated mitochondrial genes and only 15 upregulated genes. In particular, there was a notable downregulation of genes involved in the electron transport chain of the inner mitochondrial membrane, specifically in complex I (NDUF family), complex II (SDH family), complex III (UQCR), complex IV (COX), and complex V (ATP5 family) (Figure 4C, inset) as fibrosis progressed. This implies that mitochondrial functions may be less affected by liver steatosis at the early stages of MASLD but become impaired as fibrosis advances. Overall, these pronounced gene expression changes indicate impaired respiratory functions, oxidative stress, and diminished ATP production with disease progression, which could favor the exacerbation of steatohepatitis (10).

Integrative network analysis reveals significant links between liver fibrosis and its underlying gene expression alterations

To characterize the progression from steatosis to fibrosis from an integrative omics perspective, we conducted a partial correlation network analysis for liver transcriptomic, liver metabolomic, and clinical data. The network revealed that steatosis is primarily correlated with metabolites, whereas fibrosis is most closely linked to the transcriptional network (Figure 5A), indicating distinct pathological processes. To further explore representative gene signatures in the development of fibrosis, we prioritized 213 genes as markers by comparisons of gene expression levels against two different baselines (no pathology and steatosis; details provided in the methods). Notably, 75 of these markers overlapped with fibrosis-associated genes in the VA cohort and 35 overlapped with the EU cohort (Figure 5B) (20), with 130 markers being novel. Pathway analysis of these fibrosis markers highlighted prominent roles for signal transduction and ECM organization/disassembly, as

expected (Figure 5C). Moreover, by mapping fibrosis-associated genes to well-established fibrosis pathways, we identified dysregulated genes involved in ECM modulation and key fibrogenic signaling pathways (e.g., TGF-β, Wnt, Notch, MAPK, NF-kB, FXR, PPAR, and PI3K/AKT signaling pathways) that demonstrated linear correlations with fibrosis grades (Supplemental figure 5A).

In the liver, HSC-derived myofibroblasts are the key drivers of fibrosis (31). Genes involved in TGF-β and SMAD signaling cascades, which are involved in HSC activation and fibrosis (32), were consistently upregulated with progressive fibrosis grades (Figure 5, C and D). Specifically, the expression levels of genes encoding two isoforms of TGF-β, particularly *TGFB1* and *TGFB3*, and *INHBA*, encoding an inhibin subunit, increased with fibrosis progression (Figure 5D). We also observed upregulation of direct targets of the canonical TGF-β/SMAD signaling including factors involved in ECM remodeling, such as *TIMP1*, *MMP9*, and *COL5A2*, and changes in the levels of various intracellular SMAD regulators and partners such as *CDK8*, *CTDSP2*, *HDAC1*, and *HDAC7* (Figure 5D). Genes encoding ECM proteins that trigger extracellular TGF-β activation, including *ITGAV*, *LOXL2*, *THBS1*, *MMP9*, and *MMP14* (Supplemental figure 6) (33-35), were also increased, confirming the activation of TGF-β in the development of fibrosis in obese individuals with early-stage MASLD.

GTPase signaling and regulation in the transition from steatosis to fibrosis

Given that the transition from simple steatosis to the onset of fibrosis marks a critical window for disease management, we compared gene expression profiles between patients with fibrosis accompanied by steatosis and those with steatosis but no fibrosis. Notably, GTPase signaling and its regulation emerged as the top enriched pathway in this comparison (Figure 6A). The role of GTPase signaling pathways in the

early stages of liver fibrosis has not been systematically investigated with the exceptions of anecdotal reports (36-39). Among the 251 GTPase-related genes (Supporting data – Supplemental figure 5B), we identified 27 genes displaying positive associations with fibrosis progression, while 10 genes showed negative associations (Supplemental figure 5B). This indicates a potential role of GTPase signaling pathways in the development of liver fibrosis.

Interactome of GTPases and their regulators

To better understand the involvement of GTPases in fibrosis development, we focused on 251 GTPases, GTPase-activating proteins (GAPs) and guanine nucleotide exchange factors (GEFs), and examined their interactome using the human cell map (40) and a protein-protein interaction network (41, 42). There are 6,971 proteins that have been tested for physical interaction or subcellular proximity with GTPase-related genes, and 508 of these show significant associations with fibrosis progression in our cohort (Figure 6B). The network shows that GTPases and their regulators interact with a wide range of fibrosis genes, where *RAC1* and *ARF3* are the central hubs of the network. As expected, functional enrichment of the core nodes revealed that the GTPase network regulates intracellular transport, actin cytoskeleton organization, exocytosis, and other biological processes during fibrosis progression (Figure 6C). Taken together, we identified that GTPases and their regulators are co-regulated with fibrosis-related genes encoding their protein interaction partners, supporting our hypothesis about a functional link between GTPases and hepatic fibrosis.

Relationship between GTPases and TGF-β

TGF-β is a well-established marker of fibrosis progression, and *TGFB1* and *TGFB3* levels were positively associated with fibrosis grades in this cohort (Figure 5D). In light of these findings, we examined the correlations between TGF-*β* genes and GTPase-

related genes. Most GTPases and their regulatory genes were co-expressed with a positive correlation to TGF-β gene expression and the progression of fibrosis (Supplemental figure 7). We also noted the upregulation of *RAC1*, *RAC2*, and *CDC42*, which are Rho-GTPases that play a crucial role in TGF-β-induced actin cytoskeletal remodeling (43). Additionally, Ras/Rab GTPases are key factors in vesicular transport and cytoskeletal regulation by modulating receptor endocytosis, Smad protein transport, and interactions with the actin cytoskeleton within TGF-β signaling (43). This GTPase family and their regulators make up a significant portion of the GTPase gene family (100 genes), with 17 genes showing significant changes (q value < 0.05) in liver fibrosis (Supporting data – Supplemental figure 5B). Specifically, *RAB5*, which is essential for TGF-β transport and endocytosis (44), is markedly upregulated in its isoform *RAB5B* as fibrosis progressed. Overall, our results suggest a potential connection between GTPases and TGF-β.

GTPase signaling and its regulation in HSCs in vivo and in vitro

As an important fibrogenic cytokine, TGF-β mediates the activation of HSCs and the crosstalk between hepatocytes, HSCs, and Kupffer cells during liver fibrogenesis (45, 46). To validate that elevated TGF-β expression results in a potential activation of GTPases in HSCs by regulating the expression of genes encoding GTPases and their regulators, we cross-referenced our data with the transcriptomic data of HSCs isolated from mouse models of acute and chronic liver fibrosis (47). As shown in Figure 7A, our human fibrosis gene signatures, particularly those involved in the transition from simple steatosis to fibrosis, exhibited a high overlap with GTPase-related genes in response to carbon tetrachloride (CCl_4) induction in mouse HSCs. Interestingly, in this acute fibrosis model, most upregulated GTPase-related genes were observed one week after CCl_4 administration, corresponding to the time point when collagen

deposition occurred (47). This upregulation pattern also persisted in the chronic model. Overall, this supports a relationship between the onset of liver fibrosis and GTPase regulation in HSCs in vivo.

We next investigated whether inhibition of GTPases by NSC23766 (Rac1 inhibitor) or ML141 (Cdc42 inhibitor) could reduce markers of fibrogenesis in an immortalized HSC cell line, the LX-2 cells. Under basal conditions, LX-2 cells cultured with NSC23766 or ML141 exhibited a marked reduction in pro-collagen secretion by ~50-60%, respectively (Figure 7B). Gene expression analysis suggested that ML141 was more effective than NSC23766 in reducing the expression of *COL1A1* and *COL1A2* (Figure 7C). Upon TGF-β stimulation, pro-collagen secretion from LX-2 cells increased by 32% (Supplemental figure 8, B and C). Despite the diminished efficacy of GTPase inhibitors in the presence of TGF-β, NSC23766 still significantly lowered procollagen secretion by 40% (Figure 7D). Taken together, these findings suggest that inhibition of GTPase activity directly inhibits collagen production and/or secretion under both healthy and profibrogenic (TGF-β) states, highlighting the potential of GTPase inhibitors in attenuating hepatic fibrosis.

Ex vivo validation of GTPase regulation in a 3D liver spheroid model

To further confirm the altered expression of GTPases and their regulators in another independent system, we employed an established model of 3D liver spheroids in which hepatic cells remain viable and functional for multiple weeks (48-50). Specifically, we co-cultured primary human hepatocytes with Kupffer and stellate cells isolated from patients with histologically confirmed MASH (51) and examined the overall expression profile of GTPase-regulated genes between our human cohort and the ex vivo system. As displayed in Figure 7E, we observed that the levels of a large group of GTPase-related genes were increased in the disease group in both human patients and the 3D

spheroid system, with an overall concordance between the two. In comparison to the lean control groups, the MASH group demonstrated an upregulation of 24 genes encoding GTPases and their regulators (Figure 7F). Strikingly, the treatment of spheroids with elafibranor, a dual PPARα/δ agonist that showed promising anti-fibrotic effects in clinical trials (52), restored the expression levels of 17 genes back to the baseline (Figure 7F). To further validate the relationship between TGF-β and GTPases, we treated MASH spheroids with recombinant TGF-β or an inhibitor of TGF-β (TGFBi, namely TP-008) and evaluated the expression levels of selected GTPase-related genes in both 3D hepatocytes co-cultured with non-parenchymal cells and hepatocyte mono-cultures. TGF-β treatment led to a significant increase in *DOCK2* expression and an increasing trend of *VAV1* levels (two GEFs for the Rho GTPase family). Notably, the increase in expression of GEFs was reversed by the TGF-β inhibitor (Figure 7G). In contrast, *RHOU* and *RAB32* expression were mildly suppressed by TGF-β at the transcript level. Taken together, TGF-β stimulation leads to an increased expression of GEFs in ex vivo human liver spheroids and potentially regulates GTPase activity (Supplemental figure 9).

Discussion

In this study, we performed a comprehensive omics-driven analysis of a cohort of 109 obese individuals with early MASLD. Through our multi-omics analysis, we pinpointed distinct molecular features underlying steatosis and fibrosis progression in an integrative network and highlighted potential targets for early disease intervention.

Our work reinforces key findings from other studies comparing early MASLD, including altered TAG metabolism, mitochondria function, and oxidative stress (53-55). We found that the degree of steatosis in the early stage of the disease was related to the abundance of TAG and DAG in the liver. However, as the level of steatosis

increased, the level of liver sphingolipids showed a downward trend, which contrasts with previous reports of animal studies (14, 56). This reflects the likely differences in sphingolipid metabolism with increasing steatosis and/or differences between humans and mice, and aligns with the apparent discrepancy in alteration patterns for SM and ceramides across different patient cohorts (13, 14, 57). We also identified a positive correlation between dysregulation of mitochondrial lipid metabolism and aggravation of oxidative stress in hepatocytes. It is noteworthy that the increase of taurine and vitamin E, both of which have antioxidant effects, maybe a reflection of the liver's response to lipotoxicity (58, 59). These alterations in metabolism were not observed in plasma, and the liver and plasma metabolome were largely independent of each other. Therefore, one has to wonder whether conventional blood analyses will ever be accurate in identifying MASLD progression at early stages. The emergence of liquid biopsies and the evaluation of liver-specific extracellular vesicles might open up new minimally invasive diagnostic opportunities (60).

To understand the potential molecular drivers underpinning the remodeling of liver lipid metabolism in the early stage of MASLD, we analyzed the expression of genes known to regulate these metabolic pathways. The results demonstrated that extensive changes in the expression of a broad range genes that encode key enzymes of altered lipid metabolites that were detected in our metabolomic analysis. For example, changes in *DGAT2*, *PNPLA3*, and *PLIN3* expression were closely related to altered levels of TAG and DAG. The increased expression of *DGAT2*, which encodes a key enzyme catalyzing the last step of de novo TAG synthesis, implies enhanced integration of TAGs into LDs in the endoplasmic reticulum, which presumably alleviates lipid-induced ER stress and prevents the accumulation of lipotoxic lipids (Figure 4C) (61). Upregulation of *PLIN3* was correlated with higher grades of both fibrosis and steatosis. The protein encoded by *PLIN3*, along with other PLIN proteins

(62), plays an important role in LD stabilization and the prevention of TAG hydrolysis, thus potentially contributing to hepatic steatosis (63). The expression of genes involved in glycerophospholipid metabolism also changed significantly, such as *LPCAT1*, *PLD*, *ETNK2*, and *PCYT2*. With the progression of liver fibrosis, the expression levels of genes involved in primary bile acid biosynthesis, PUFA metabolism, and steroid hormone biosynthesis decreased, especially *ACADS*, *ACADSB*, and *ACADM* which encode key enzymes in the initial stage of catalyzing fatty acid β-oxidation, and *HADH* and *ACAA1*, which encode enzymes that act in the late stage of β-oxidation (64). Further exploration found that as fibrosis progressed, significantly more mitochondrial genes were downregulated, especially genes related to the electron transport chain of the mitochondrial inner membrane. This may indicate that pathological oxidative stress and energy metabolism caused by early mitochondrial dysfunction may aggravate fatty liver inflammation (65), and the aggravation of the inflammatory response may become an important cause of liver fibrosis.

GTPase signaling is known to regulate several biological processes (66). Previous studies have unveiled that Rho-, Rap-, and Rab-GTPases play a role in lipogenesis, pathogenesis, and lipophagy in the liver (36-39); however, little attention has been paid to their roles in early fibrosis formation. Our study found that a number of GTPase-related genes were upregulated with the emergence and progression of fibrosis. Correlation analysis indicated that expression levels of GTPase-related genes were associated with TGF-β gene expression. *RAB32*, as the only RAB protein associated with mitochondria, was significantly upregulated in our study. Previous studies have shown that knocking down *Rab32* can reduce the accumulation of intracellular lipids in hepatocytes (67). In particular, it has been reported that Rho GTPase family acts as a key factor in the progression of fibrosis, especially *RAC2* and

CDC42 (68, 69). *RAC2* is involved in regulating the expression of inflammatory cytokines and chemokines (68), and it also participates in regulating the reorganization of the cytoskeleton with *RHOU* and *ARHGAP30*—also small GTPases of the Rho family—affecting cell morphology, movement and adhesion. In the 3D spheroid MASH system, elevation of GTPase regulators was observed, but treatment with elafibranor restored their expression to baseline levels. Elafibranor has demonstrated promising effects against insulin resistance, inflammatory effects, and fibrosis via dual-inhibition of PPARα/δ. In an international, randomized, double-blind placebo-controlled clinical trial, Elafibranor effectively resolved steatohepatitis and reduced liver fibrosis stages in patients with MASH, indicating a potent anti-fibrotic effect (52). The downregulated expression of GTPase regulators following elafibranor treatment suggests a potential anti-fibrotic mechanism involving GTPase signaling. Additionally, in this spheroid model, we identified the upregulated expression of GEFs (*VAV1* and *DOCK2*) for Rac/Rho upon TGF-β stimulation. Notably, the Rac inhibitor, NSC23766, showed a significant effect in reducing pro-collagen secretion from HSC LX-2 cells in the presence or absence of TGF-β. Based on the results from the two independent experiments, we thus discovered a novel role of Rac/Rho GTPases in liver fibrogenesis in MASLD patients through the mechanism of TGF-β-induced actin cytoskeleton remodeling (43). In summary, we validated the omics-driven findings from the human cohort using both an in vitro system and an ex vivo spheroid model, highlighting the translational value of GTPase-targeting strategies.

GTPases have already been explored as drug targets in other diseases. For instance, sotorasib, a KRAS inhibitor, was recently approved by the FDA for the treatment of non-small-cell lung cancer (70). More recently, Morstein et al. identified a conserved cryptic pocket that allows small molecule probes or drugs to target Ras-, Rho-, and Rab-family GTPases (71). The discovery of novel druggable targets among

small GTPases has further strengthened the feasibility of GTPase inhibition as a potential therapeutic strategy to prevent the progression of early MASLD development to irreversible fibrosis.

Overall, our study delineated the molecular profiles of obese individuals with early-stage MASLD and identified GTPase signaling as a potential driver of fibrosis in MASLD, which could provide new avenues for therapeutical approaches.

Materials and Methods

Cohort recruitment and ethic approval

Participants provided written and verbal informed consent. The study protocol conforms to the ethical guidelines of the 1975 Declaration of Helsinki and was approved by the University of Melbourne Human Ethics Committee (ethics ID 1851533), The Avenue Hospital Human Research Ethics Committee (Ramsay Health; ethics ID WD00006, HREC reference number 249), the Alfred Hospital Human Research Ethics Committee (ethics ID GO00005), and Cabrini Hospital Human Research Ethics Committees (ethics ID 09-31-08-15).

Eligible patients with obesity scheduled for primary or secondary sleeve gastrectomy, gastric bypass, or the insertion of a laparoscopic-adjustable band were prospectively enrolled. Details of inclusion and exclusion criteria and clinical laboratory assays are provided as supplementary information.

Liver biopsy collection and histological feature assessment

An ~ 1 cm^3 wedge liver biopsy was collected from the left lobe of the liver during surgery. The liver was cut into two portions. One portion was placed in formalin and transported to TissuPath^{TM} (Mount Waverley, Victoria), paraffin embedded and processed for histological analysis. Samples were graded according to the Clinical Research Network NAFLD activity score [NAS] (72) and Kleiner classification of liver fibrosis (73) by a liver pathologist at TissuPath. Patients with no pathology were defined by steatosis score of 0, regardless of inflammation or fibrosis grade 1. MASL patients were defined by a steatosis score ≥1 with or without lobular inflammation. MASH was defined joint presence of steatosis, lobular inflammation, and ballooning. The remainder of liver samples was utilized for the metabolite secretome experiment, with details provided in the supplementary file.

Metabolomics data acquisition and processing

Sample preparation process for untargeted metabolomic analysis is described in the supplementary file. A 1 μL aliquot of the extract was subjected to LC-MS analysis using the Sciex TripleTOF 6600 system coupled with the Agilent 1290 HPLC. Both reverse phase and hydrophilic interaction liquid chromatography columns were used for chromatographic separations of lipids and polar metabolites, respectively. For the analysis of aqueous fraction, metabolites were separated on SeQuant ZIC-cHILIC (3 μm, 100Å, 100x2.1 PEEK) column with a flow rate of 0.25 mL/min in a 24-minute run. For lipid analysis, samples in organic phases were separated on RRHD Eclipse Plus C18 (2.1 x 50 mm, 1.8 μm). Details of LC methods are provided in the supplementary file.

Data acquisition was performed in both positive and negative ionization modes. Data-dependent acquisition (DDA) was performed on pooled samples for compound identification and SWATH-MS analysis was applied to individual samples for relative quantification. Data was converted into mzML format and was then processed by MetaboKit (74). To gain broad metabolite coverage, we curated a data processing pipeline for metabolites identified via spectral matches (MSMS-level) and those identified solely through mass matches (MS1-level). For metabolite quantification, the project-specific spectral library generated from DDA analysis was used to extract MS1 and MS2 features from the SWATH data using the MetaboKit DIA module. Compound transitions with a coefficient of variation > 30% were excluded from the analysis. For each compound, the transition with the lowest coefficient of variation and an adequate detection rate across samples was chosen as the quantifier. Metabolites that were detected in CM but not in the liver were removed from the CM metabolome.

RNA sequencing

Transcriptome sequencing service was provided by Biomarker Technologies (BMK), GmbH. Briefly, RNA were extracted from liver biopsies using Trizol reagent. The quality and quantity of extracted RNA was assessed by Nanodrop (quantity and purity) and Labchip GX (Quality). The cDNA libraries were prepared using Hieff NGS Ultima Dual-mode mRNA Library Prep Kit from Illumina (Yeasen) as per manufacturer's instructions. RNA sequencing was performed on NoveSeq6000 platform (PE 150 mode).

For raw data processing, FastQC (v0.11.9) was used as a quality control check for raw sequencing. Alignment to the reference genome (GRCh38, Ensembl release 77) was performed using STAR (v2.7.9a), and gene expression levels (transcripts-per-million, TPM) were estimated using RSEM (v1.3.1). Gene expression data underwent a logarithmic transformation to log2(TPM + 1) and mean-centring normalization for downstream analyses.

Statistical analysis

All analyses in this study were conducted using R version 4.3.1. Linear regression model was used to evaluate the linear association between histological grades and molecular abundance levels with adjustment for age, gender, BMI, and diabetes. Statistically significantly changed metabolites or genes were defined by controlling the overall type I error at 5% or 10% (q value < 0.05 or 0.1). Gene overrepresentation analyses were performed using gene ontology recourse by in-house software (75). ClueGO, a plugin app in Cytoscape, was used to visualize enrichment maps (76). Partial correlation network analysis was employed to integrate the two omics layers using an in-house partial correlation network algorithm ACCORD. KEGG pathway database was used for the analysis of lipid metabolism (77). All network visualizations in this study were done using Cytoscape (78).

To identify progressive markers of liver fibrosis, we performed pairwise analyses for fibrosis stages using two distinct baselines: patients with no pathology and those with steatosis and without fibrosis. 213 markers were characterized as progressive based on the following criteria: a) significant linear association with fibrosis grades, and b) significant differential expression (p value < 0.05 in t-test) in at least two fibrosis stages (e.g., F1 and F2, F2 and F3) compared to both baselines.

For meta-analysis of reference human cohorts, the two RNA-seq datasets of the liver transcriptome, the VA cohort (GSE130970) and the EU cohort (GSE135251), were downloaded from Gene Expression Omnibus, and associations between gene expression (log2 TPM) and fibrosis grades or NAS were analysed using linear regression. In the EU cohort, the patients without MASH diagnosis were removed from the meta-analysis for the purpose of identifying fibrosis signatures in MASH patients.

Cross-referencing datasets of mouse models

The RNA sequencing data (raw counts) for HSCs isolated from liver fibrosis mouse models (47) was downloaded from GSE176042 and analyzed using the DESeq2 R package. This previously published study investigated HSC initiation and perpetuation using acute and chronic models, respectively. For the acute model, mice were injected with CCl_4 once and samples were taken at 24 h, 72 h, and 1 w. For the chronic model, mice received a regimen of semi-weekly injection of CCl_4 for 4 weeks. After this regimen, mice were sacrificed and samples were taken at 24 h, 72 h, and 2 w.

In vitro validation in LX-2 cells

LX-2 human hepatic stellate cells (# SCC064) were purchased from Merck. LX-2 cells were maintained in high glucose DMEM, supplemented with 2% fetal bovine serum (FBS). LX-2 cells were supplemented with 1% pencillin-streptomycin and 1X Glutamine (Millipore Cat. No. TMS-002-C) unless specified otherwise. All cells were

maintained in a humidified incubator at 37°C and 5% CO_2. Cells were seeded at a density of 500,000 for 12 well plates in high glucose DMEM, supplemented with 10% FBS for 24 h. The cells were then serum starved in high glucose DMEM for 24 h and then incubated with high glucose DMEM with either established IC50 doses of NSC23766 at 100μM (MedChemExpress) and ML141 (MedChemExpress) with or without 5ng/mL of TGFβ1 (R&D systems) for 24 h. The supernatant was collected, centrifuged at 300 x g for 10 min and snap frozen in liquid nitrogen for assessment of secreted collagens. The cell lysate was washed with ice-cold PBS three times, lysed in 1 mL of Trizol reagent (Gibco), and snap-frozen in liquid nitrogen for mRNA assessment. RNA extraction and qPCR test procedures are provided in the supplementary file.

Human procollagen secretion was measured using the Human Pro-collagen 1A1 ELISA kit (R&D Systems, cat. no. DY6220-05) and Ancillary Reagent Kit DY008B (R&D Systems, cat. no. DY6220-05). Briefly, cell supernatants were thawed on ice, and an aliquot was diluted by a factor of 1:100 (v:v) and assessed according to the manufacturer's instructions.

3D liver spheroid MASH model

3D liver spheroids were generated based on co-cultures of cryopreserved primary human hepatocytes (PHH) and liver non-parenchymal cells (NPC) as previously described (51). Briefly, cells were seeded at a PHH:NPC ratio of 6:1 in 96-well ultra-low attachment plates (CLS7007-24EA Corning) with a total of 1500 cells/well in culture medium (William's E medium containing 11 mM glucose, 100 nM dexamethasone, 10 μg/mL insulin, 5.5 mg/L transferrin, 6.7 μg/L selenite, 2 mM L-glutamine, 100 U/mL penicillin, 0.1 mg/mL streptomycin) supplemented with 10% FBS. After spheroid formation FBS was phased out and cells were maintained in

medium supplemented with albumin-conjugated free-fatty acids (FFA) including 80μM palmitic acid and 80 μM oleic acid. At the end of the experiment, spheroids were collected for RNA extraction (Zymo R105). The elafibranor treatment protocol was described in the previous study (51).

For the TGF-β stimulation and inhibition experiment, PHH-NPC spheroids in the treatment groups were exposed to either TGF-β1 at 10 ng/ml or 5 μM of the TGF-β inhibitor TP008 for one week with media changes every 2-3 days. Expression of the selected genes was evaluated using Fluidigm qPCRs. Gene expression was reported as fold change compared to the control group and genes were normalized to GAPDH. For the qPCR analysis, ordinary one-way ANOVA was used for statistical analysis.

Data availability

All data are available within the manuscript, supporting data values, and the supplementary file. RNA sequencing data to this article have been submitted to SRA (PRJNA1185558) and is deposited with GEO (GSE281797). Untargeted LC-HRMS data is deposited with Zenodo, including IDA data (DOI 10.5281/zenodo.14091962), SWATH data for the organic fraction (DOI 10.5281/zenodo.14096635), and SWATH data for the aqueous fraction (DOI 10.5281/zenodo.14096753, DOI 10.5281/zenodo.14136832).

Funding

PK is supported in part by the Swedish Research Council (2021-01331), the Swedish Cancer Society (Cancerfonden; 21-1566Pj), the Crafoord Foundation (Ref. No. 20220628), the Swedish Foundation for Strategic Research Dnr IRC15-0067, and Swedish Research Council, Strategic Research Area EXODIAB, Dnr 2009-1039. LNZ is supported in part by the IngaBritt och Arne Lundbergs Forskningsstiftelse LU2020-

0013, the Crafoord Foundation (Ref. No. 20210516, Ref. No. 20220582), Stiftelsen Längmanska kulturfonden (BA21-0148), and the Åke Wibergs Stiftelse. VML acknowledges support from the Swedish Research Council (2021-02801 and 2023-03015), the Ruth och Richard Julins Foundation for Gastroenterology (2021-00158), Knut and Alice Wallenberg Foundation (VC-2021-0026), by the SciLifeLab and Wallenberg National Program for Data-Driven Life Science (WASPDDLS22:006), a Novo Nordisk Pioneer Innovator Grant (NNF23OC0085944), the Robert Bosch Foundation, as well as the Innovative Medicines Initiative 2 Joint Undertaking (JU) under grant agreement No. 875510. The JU receives support from the European Union's Horizon 2020 research and innovation programme and EFPIA, Ontario Institute for Cancer Research, Royal Institution for the Advancement of Learning McGill University, Kungliga Tekniska Hoegskolan, and Diamond Light Source Limited. HC is supported in part by Singapore Ministry of Education (T2EP202121-0016, T2EP20223-0010), National Research Foundation and Agency for Science, Technology and Research (I1901E0040), and National Medical Research Council (CG21APR1008). MJW is supported by the National Health and Medical Research Council of Australia (APP1162511). The funders had no role in study design, data collection and interpretation, or the decision to submit the work for publication.

Acknowledgments

We thank all present and past members of the Watt, Choi, Lauschke, Kaldis laboratories for discussions, input, and support.

Conflict-of-interest statement

VML is co-founder, CEO and shareholder of HepaPredict AB, as well as co-founder and shareholder of Shanghai Hepo Biotechnology Ltd. All other authors declare no conflict of interest.

Author contributions

QZ*: designing research studies, conducting experiments, acquiring data, analyzing data, writing the manuscript
WD*: designing research studies, conducting experiments, acquiring data, analyzing data, writing the manuscript
RW*: analyzing data, writing the manuscript
YZ: conducting experiments, acquiring data, analyzing data
UK: analyzing data, writing the manuscript
LNZ: analyzing data, writing the manuscript
HT: conducting experiments, acquiring data, analyzing data
SY: conducting experiments, acquiring data, analyzing data
MY: conducting experiments, acquiring data, analyzing data
YX: conducting experiments, acquiring data, analyzing data
YK: conducting experiments, acquiring data, analyzing data
SL: conducting experiments, acquiring data, analyzing data
RL: conducting experiments, acquiring data, analyzing data
GT: conducting experiments, acquiring data, analyzing data
PN: conducting experiments, acquiring data, analyzing data
PRB: providing reagents, cohort management
VMK: designing research studies, analyzing data, writing the manuscript, supervision, funding acquisition
HC: designing research studies, analyzing data, writing the manuscript, supervision, funding acquisition
MJW: designing research studies, analyzing data, writing the manuscript, supervision, funding acquisition
PK: designing research studies, analyzing data, writing the manuscript, supervision, funding acquisition, leading of collaboration

QZ, WD, and RW are co-first authors based on their contributions, which was LC-MS data acquisition and bioinformatic analysis of transcriptomic, metabolomic, and clinical data (QZ), organizing cohort samples, clinical parameters, managing, and LX-2 experiments (WD), and writing the original draft and analyzing data (RW).

Abbreviations

CCl_4 Carbon tetrachloride
CM Conditioned medium
CYP Cytochrome P
DAG Diacylglycerol
ECM Extracellular matrix
GAP GTPase-activating protein
GEF Guanine nucleotide exchange factor
GL Glycerolipid
HSC Hepatic stellate cell
LD Lipid droplet
MASH Metabolic dysfunction-associated steatohepatitis
MASLD Metabolic dysfunction-associated steatotic liver disease
NAS NAFLD activity score
PCA Principal component analysis
SM Sphingomyelin
Vitamin E Alpha-tocopherol
TAG Triacylglyceride
GPL Glycerophospholipid
PUFA Polyunsaturated fatty acid

1 **Table 1. Patient characteristics**

	Patients (n)	No Pathology (N = 33)	MASL (N = 65)	MASH (N = 11)	P value
Age (median (MAD)	109	36 (14.83)	41 (8.9)	43 (14.83)	0.925
Gender = Male (%)	108	4 (12.1)	17 (26.6)	5 (45.5)	0.062
Diabetes = Yes (%)	109	2 (6.1)	25 (38.5)	2 (18.2)	0.002
Hypertension = Yes (%)	93	6 (18.2)	13 (26.5)	3 (27.3)	0.653
BMI (median (MAD)	108	42.61 (6.6)	44.55 (9.79)	44.52 (7.16)	0.08
ALT (median (MAD)	104	24 (11.86)	39.5 (22.24)	65 (34.1)	0.668
AST (median (MAD)	104	24 (7.41)	29 (11.86)	45 (26.69)	0.421
ALT/AST (median (MAD)	104	1 (0.31)	1.29 (0.38)	1.37 (0.41)	0.021
GGT (median (MAD)	104	23 (10.38)	28 (12.6)	27 (13.34)	0.105
eGFR (n (%))	103	42.61 (6.6)	44.55 (9.79)	44.52 (7.16)	0.563
> 90		23 (79.3)	45 (71.4)	8 (72.7)	
60 - 90		5 (17.2)	17 (27.0)	2 (18.2)	
< 60		1 (3.4)	1 (1.6)	1 (9.1)	
Total cholesterol (median (MAD)	104	4 (0.89)	4.2 (1.04)	4 (1.33)	0.199
HDL (median (MAD)	102	1.04 (0.19)	0.93 (0.19)	0.95 (0.15)	0.151
LDL (median (MAD)	101	2.2 (0.74)	2.6 (0.74)	2.3 (1.04)	0.199
Non-HDL cholesterol (median (MAD)	108	2.76 (0.92)	3.28 (1)	3 (1.33)	0.012
Blood triglyceride (median (MAD)	103	1.2 (0.59)	1.5 (0.52)	1.6 (0.59)	0.035
Insulin (median (MAD)	100	7.95 (5.63)	9.6 (6.52)	17.7 (14.23)	0.05
FBG (median (MAD)	102	4.9 (0.74)	5.2 (0.96)	5 (0.74)	0.287
C-peptide (median (MAD)	101	0.8 (0.39)	1.08 (0.4)	1.25 (0.67)	0.001
HOMA2 - %B (median (MAD)	92	101.95 (52.11)	121 (70.57)	158.3 (31.43)	0.235
HOMA2 - %S (median (MAD)	92	88.3 (51.97)	74.4 (46.41)	33.6 (14.83)	0.053
HOMA2 – IR (median (MAD)	92	1.13 (0.74)	1.34 (0.83)	2.98 (1.02)	0.028
Steatosis (n (%))	109				<0.001
0		33 (100.0)	0 (0.0)	0 (0.0)	
1		0 (0.0)	40 (61.5)	1 (9.1)	
2		0 (0.0)	20 (30.8)	7 (63.6)	
3		0 (0.0)	5 (7.7)	3 (27.3)	
Inflammation (n (%))	109				<0.001
0		30 (90.9)	21 (32.3)	0 (0.0)	
1		3 (9.1)	40 (61.5)	6 (54.5)	
2		0 (0.0)	3 (4.6)	4 (36.4)	
3		0 (0.0)	1 (1.5)	1 (9.1)	
Ballooning (n (%))	109				<0.001
0		33 (100.0)	65 (100.0)	0 (0.0)	
1		0 (0.0)	0 (0.0)	10 (90.9)	
2		0 (0.0)	0 (0.0)	1 (9.1)	
NAS (n (%))	109				<0.001
0		30 (90.9)	0 (0.0)	0 (0.0)	
1		3 (9.1)	15 (23.1)	0 (0.0)	

2		0 (0.0)	29 (44.6)	0 (0.0)	
3		0 (0.0)	13 (20.0)	0 (0.0)	
4		0 (0.0)	8 (12.3)	6 (54.5)	
5		0 (0.0)	0 (0.0)	2 (18.2)	
6		0 (0.0)	0 (0.0)	2 (18.2)	
7		0 (0.0)	0 (0.0)	1 (9.1)	
Fibrosis (n (%))	109				<0.001
0		27 (81.8)	20 (30.8)	3 (27.3)	
1		6 (18.2)	25 (38.5)	2 (18.2)	
2		0 (0.0)	17 (26.2)	3 (27.3)	
3		0 (0.0)	3 (4.6)	3 (27.3)	

MASL: Metabolic dysfunction-associated steatotic liver; MASH: Metabolic dysfunction-associated steatohepatitis; MAD: Median absolute deviation; BMI: Body mass index; ALT: Alanine transaminase; AST: Aspartate aminotransferase; GGT: Gamma-glutamyl transpeptidase; eGFR: Estimated glomerular filtration rate; HDL: High-density lipoprotein; LDL: low-density lipoprotein; FBG: Fasting plasma glucose; HOMA2 – B: Homeostatic model assessment 2 of Beta-cell function; HOMA2 – S: Homeostasis model assessment 2 of insulin sensitivity; HOMA2 – IR: Homeostasis model assessment 2 of insulin resistance; NAS: Nonalcoholic fatty liver disease activity score.

1 **Graphical abstract**

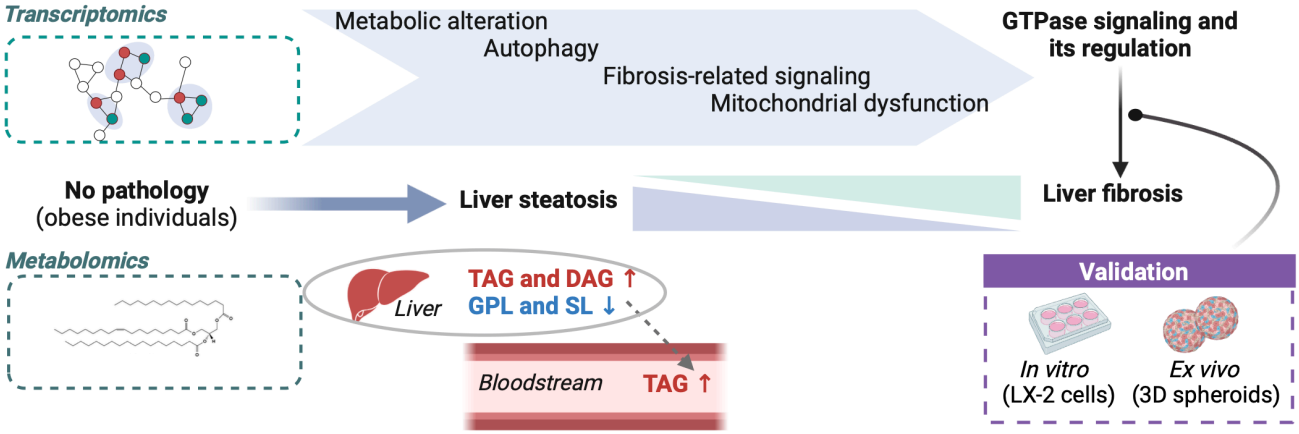

2
3

Figures

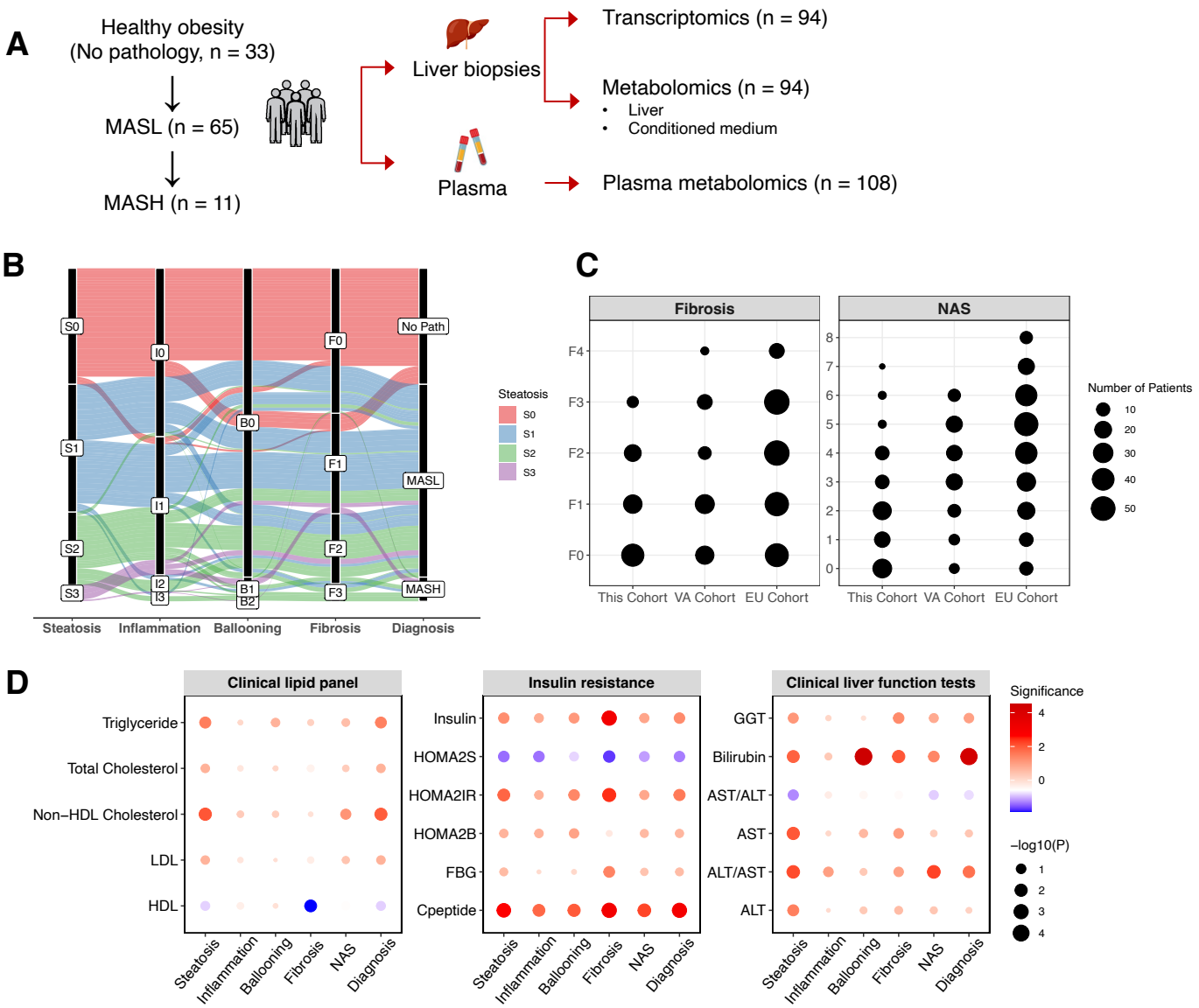

Figure 1: Study design and an overview of obese study participants. (A) The overall study design. (B) Alluvial diagram of patient composition of groupings across liver histological features. (C) Disease spectra covered in this cohort and two published datasets. (D) Relationship between clinical test results and stages of liver histological features. Node size was determined by –log10(p value) in ANOVA tests. Color indicates the significance degree [–log10(p value)] and the direction of change from early to late stages. Diagnosis: No pathology, MASL, or MASH.

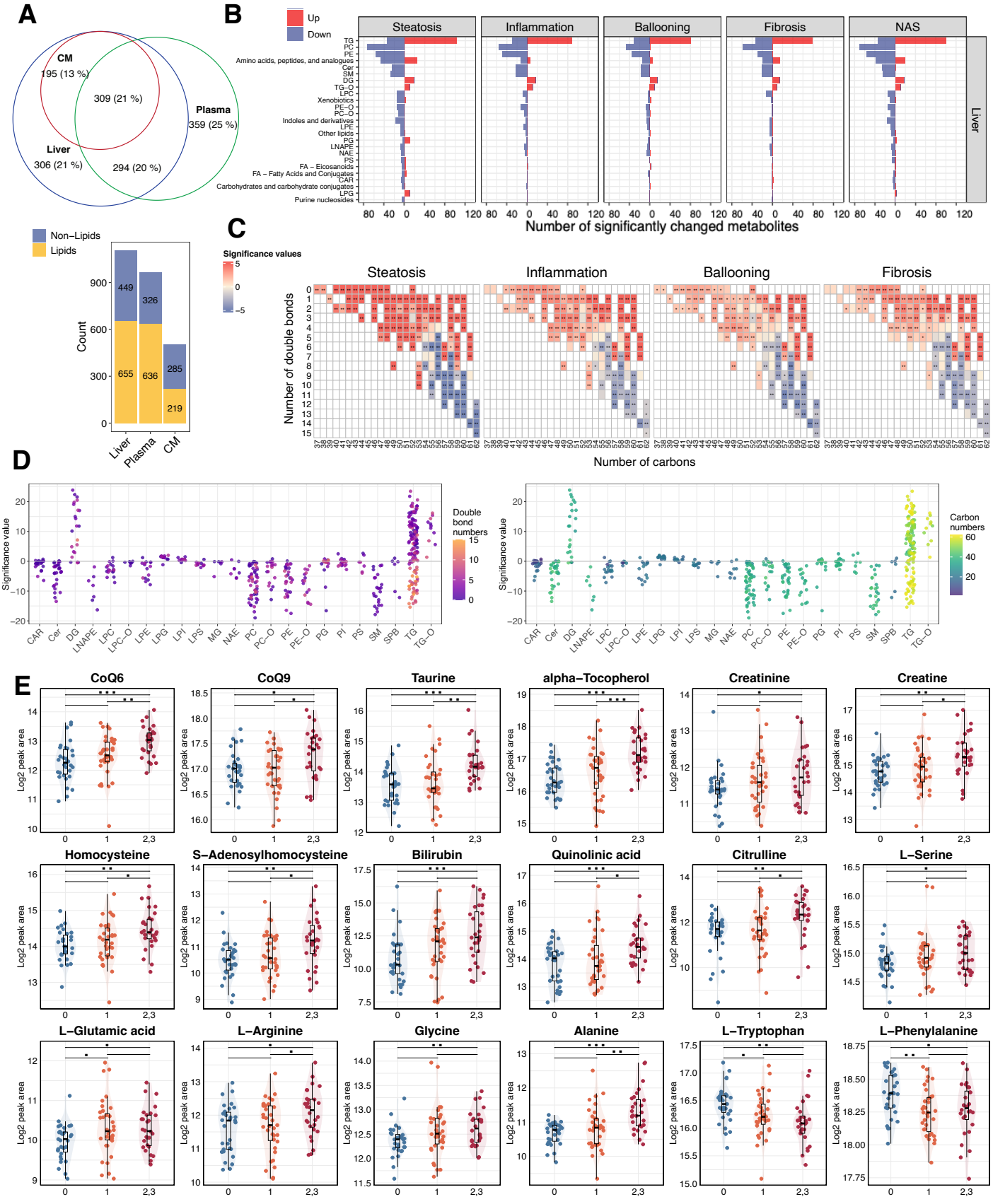

Figure 2: Metabolomic profiling of liver biopsies, plasma, and conditioned medium. (A) Venn diagram of metabolites analyzed in the liver, plasma, and conditioned medium. (B) Number of metabolites in each class that were significantly

associated with histological features in the liver (q value < 0.05). Metabolite classes with at least 5 metabolites with significance are shown in the plot. (C) Associations between fatty acid composition of triacylglycerides (TAGs) and histological outcomes. Significance values refer to –log10(p value)*sign(coefficient) from linear regression models. (D) Associations between steatosis grades and lipid species in each lipid class. Dots were colored by double bond numbers (left) and carbon numbers (right) of lipid species, respectively. (E) Metabolite alterations corresponding to the advancement of steatosis grades (x-axis).

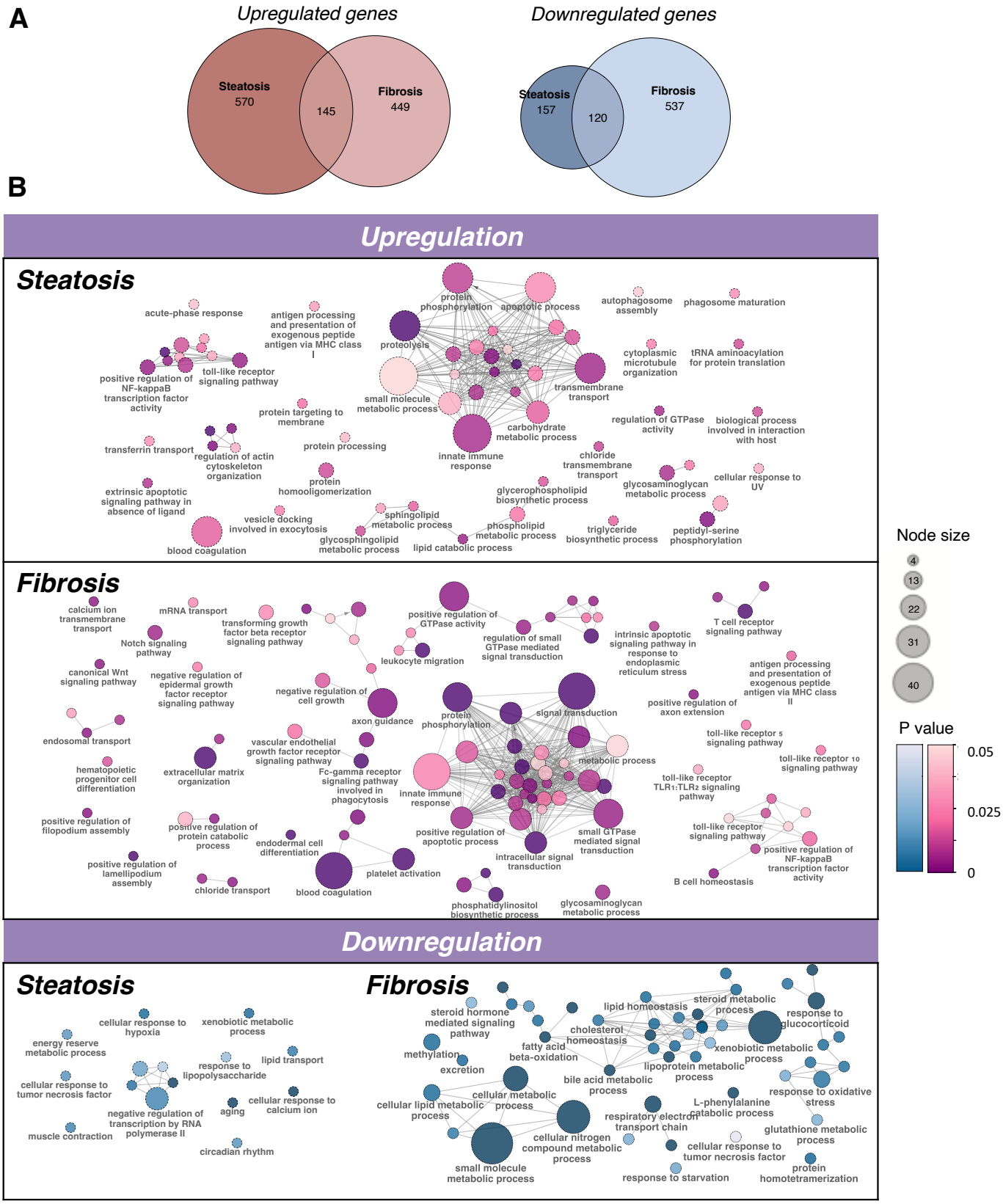

Figure 3: Characterization of gene expression profiles in obese MASLD individuals. RNA sequencing was performed on liver samples. (A) Venn diagrams depicting the number of genes significantly associated with steatosis and fibrosis (q value < 0.05). (B) Functional enrichment map illustrating the enriched biological

processes associated with steatosis and fibrosis. Node size is depicted by the largeness of the circle, while p value is indicated by color.

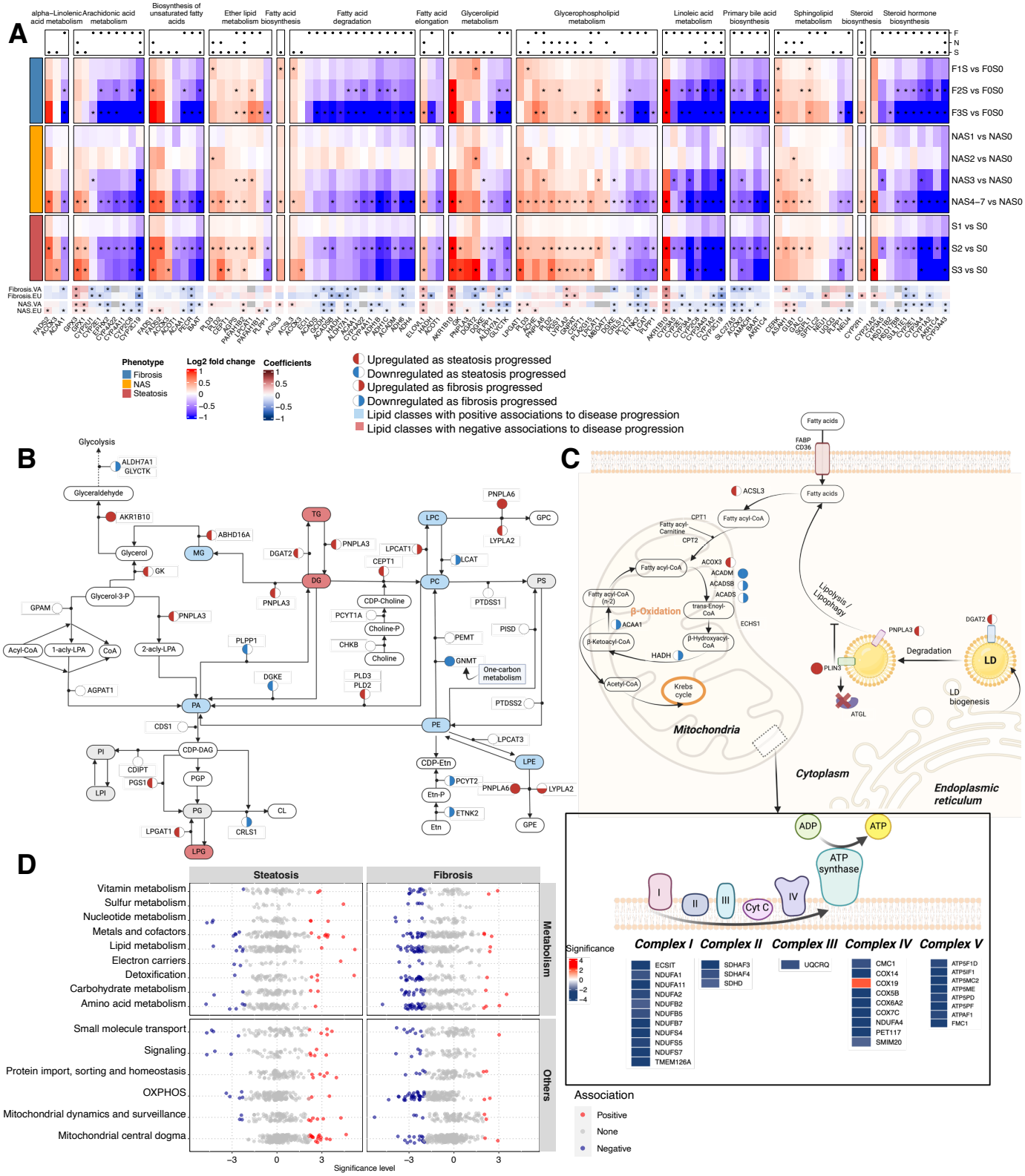

Figure 4: Lipid metabolism and mitochondrial dysfunction in the liver of obese individuals. (A) Heatmap of log2 fold changes from pair-wise analysis of lipid metabolism-related genes. Association with steatosis (S), NAS (N), and fibrosis (F) is indicated by black dots (q value < 0.05, top). Results were cross-referenced with two published cohorts (VA cohort, GSE130970; EU cohort, GSE135251) (*q value < 0.05 and with consistent direction of changes as in our cohort, bottom). (B) An integrative map of transcriptomics and metabolomics of glycerolipid and glycerophospholipid

metabolism in early MASLD. (C) Gene expression changes in fatty acid β-oxidation, mitochondrial respiratory chain, and lipid droplet (LD) metabolism associated with steatosis and fibrosis. Genes involved in respiratory electron transport were colored by the significance (–log10(p value)*sign(coefficient)) in relation to fibrosis grades. Inset: gene expression changes in the electron transport chain are depicted. (D) Gene expression regulation for metabolic pathways and mitochondria-related biological processes with statistical association to steatosis and fibrosis.

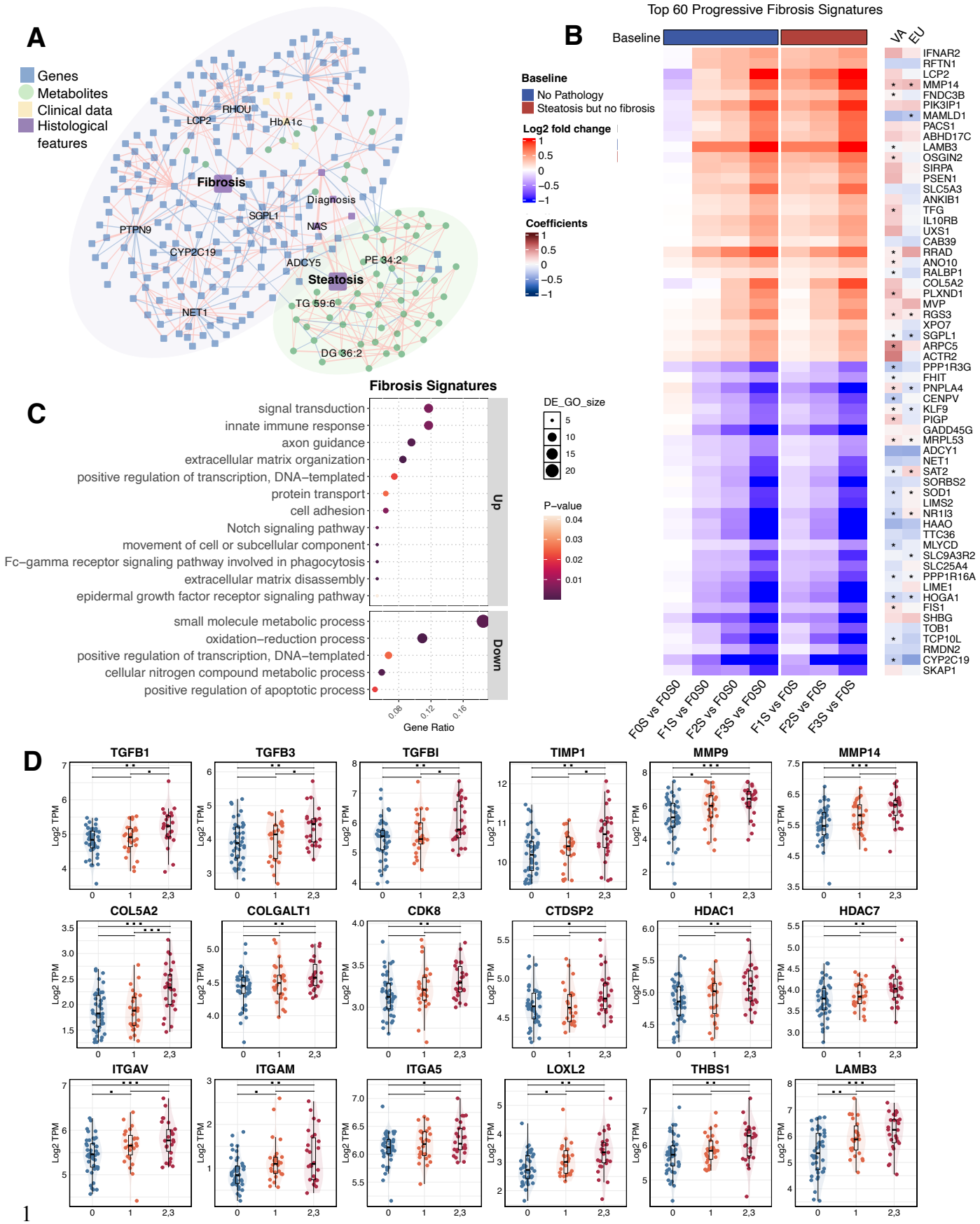

Figure 5: Liver fibrosis signatures and related pathways. (A) Network of genes, metabolites, and histological features (fibrosis and steatosis) using partial correlation analysis as described in the methods. (B) Top 60 fibrosis markers in the liver. A total

of 213 genes were identified, from which the top 30 upregulated and top 30 downregulated genes are visualized. The left side of the plot (blue bar on top) shows the comparison of patients with fibrosis and patients without pathology (baseline - “no pathology”). For the right side (red bar), patients with fibrosis were compared to those with steatosis but no fibrosis (baseline – “steatosis but no fibrosis”). (C) Pathway analysis of the enrichment of pathways for the 213 fibrosis signatures. (D) TGF-β and SMAD related gene expression associated with fibrosis grades (x-axis) is depicted. Significance is indicated by black dots; * $p < 0.05$, ** $p < 0.01$, *** $p < 0.001$.

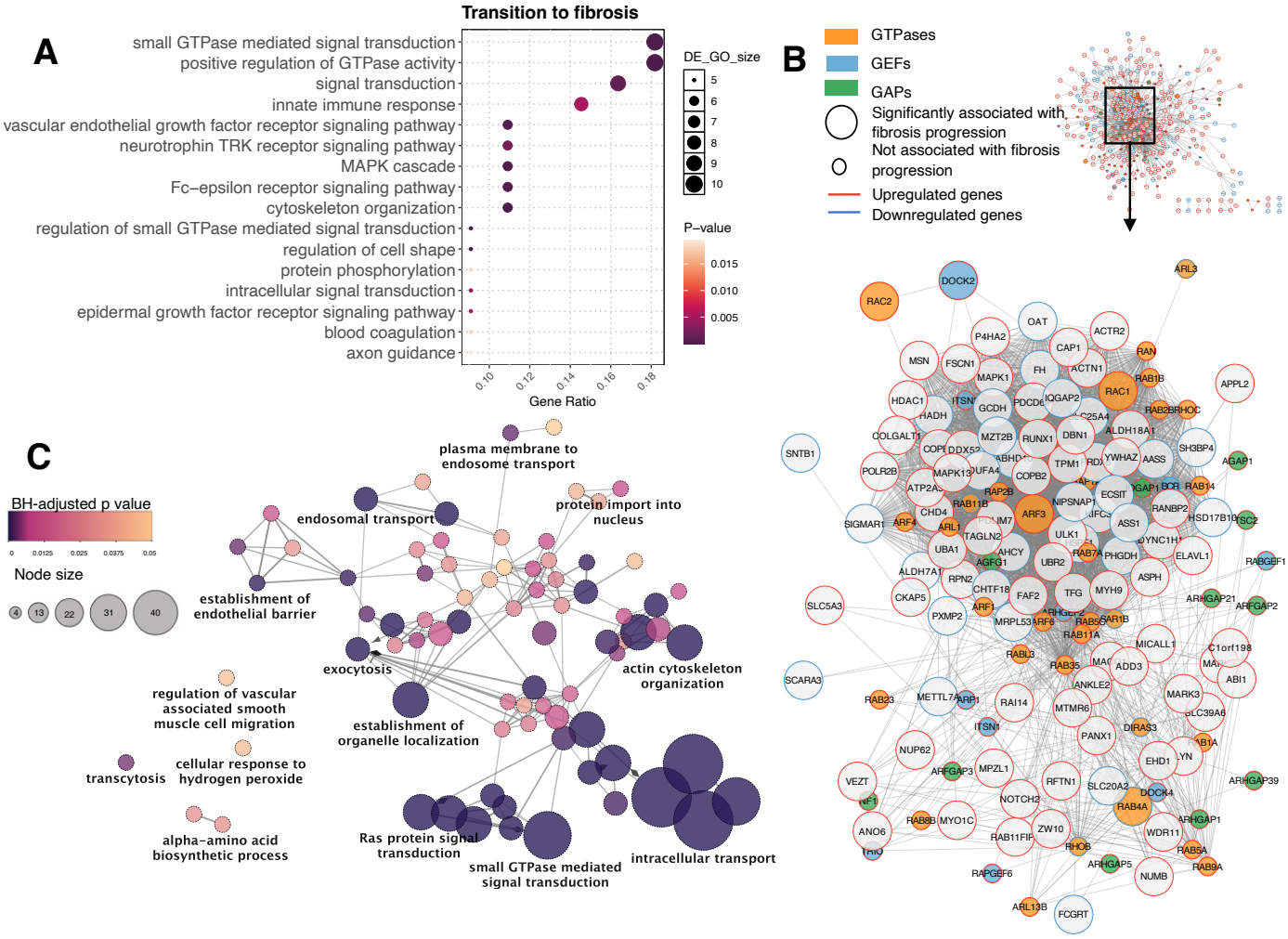

Figure 6: GTPase signaling and its regulation in liver fibrosis development in this human cohort. (A) Enrichment of pathways in the transition from simple steatosis to the onset of fibrosis. (B) Protein interaction network of GTPases and their regulators. Nodes are colored based on gene type, with borders indicating the direction of gene regulation. Node size corresponds to the significance of the genes in relation to fibrosis grades within this cohort. GEFs: Guanine nucleotide exchange factors. GAPs: GTPase-activating proteins. (C) Enrichment map of selected genes constituting the core of the network. Nodes are colored according to BH (Benjamini-Hochberg) adjusted p-value, and node sizes are proportional to the number of genes in the term.

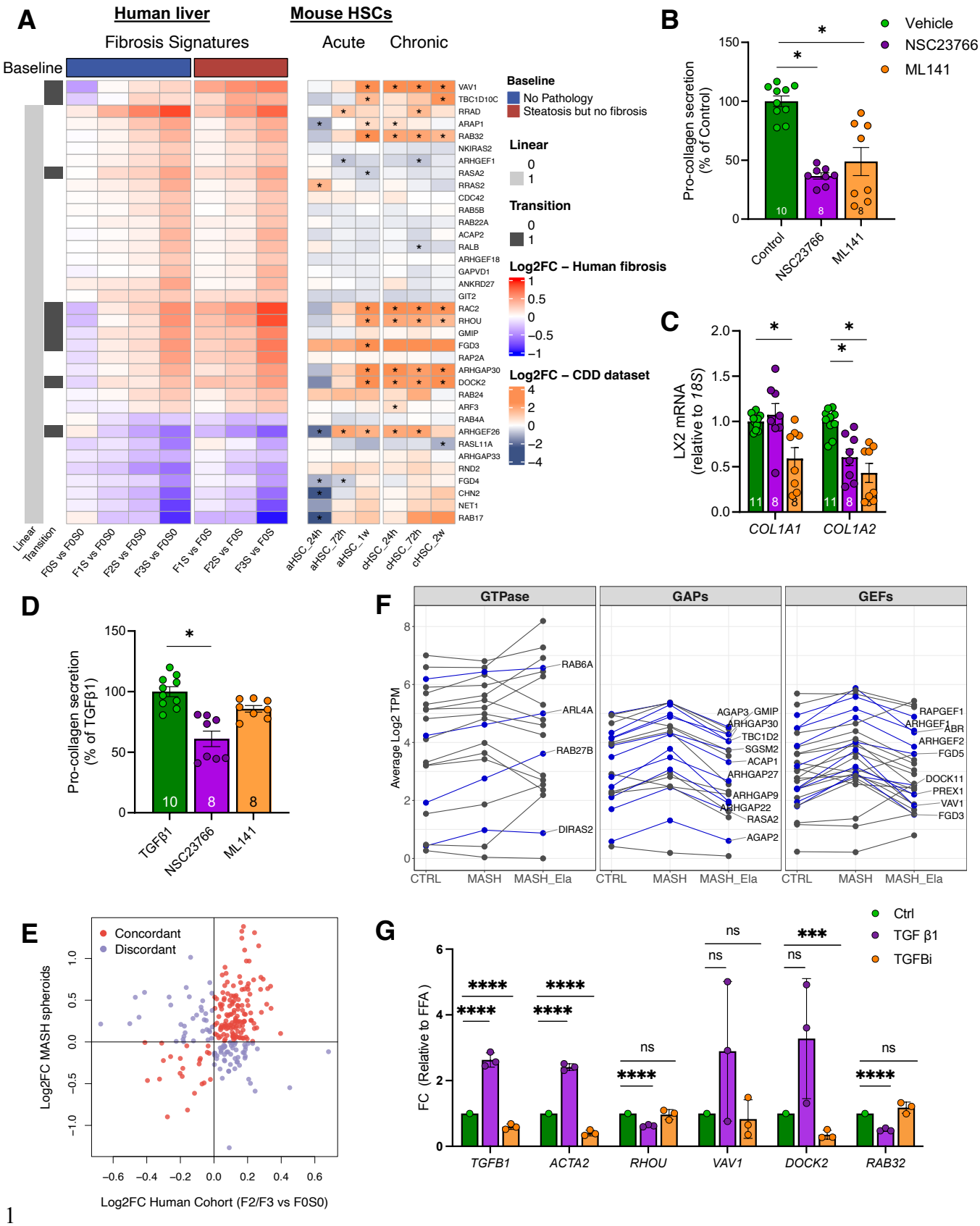

Figure 7: Validation of GTPase regulation in hepatic stellate cells and a 3D spheroid MASH model. (A) Human fibrosis signatures from the present study were partially reflected in a mouse study (GSE176042), where RNA sequencing was performed on hepatic stellate cells (HSCs) isolated from both acute and chronic mouse

fibrosis models. GTPase-related genes, especially those involved in the initiation of fibrosis, were also upregulated in HSCs isolated from both acute and chronic liver fibrosis mouse models at different time points. Row annotations *'Linear'* and *'Transition* indicate whether gene expression is linearly associated with fibrosis grades (*Linear* = 1) or shows a significant difference between patients with fibrosis and steatosis versus simple steatosis (*Transition* = 1). (B) GTPase inhibitors NSC23766 (Rac1 inhibitor) and ML141 (Cdc42 inhibitor) significantly reduced pro-collagen secretion from HSC-like LX-2 cells and inhibited gene expression of *COL1A1* and *COL1A2* (C) under basal conditions. (D) NSC23766-mediated GTPase inhibition impairs pro-collagen secretion from LX-2 cells after TGF-β treatment. Pro-collagen secretion was determined by ELISA and gene expression levels were assessed by qPCR. Asterisks (*) denote p value < 0.05 for statistical significance from one-way ANOVA with Holms-Sidak multiple comparisons (B&C) or unpaired t-test (D). (E) Comparison of expression level changes in GTPase-related genes between this human cohort and an independent 3D spheroid MASH system. Log2 fold change for the human cohort was calculated by comparing patients with grade 2 or 3 fibrosis to those without fibrosis or steatosis. Genes with the same direction of change are colored in red, while others are colored in purple. (F) Expression of GTPase-related genes in patient-derived 3D liver spheroids (controls; MASH; MASH treated with Elafibranor). Sixty-eight genes with a p-value < 0.05 from the ANOVA test were plotted in the diagram, with blue lines highlighting 24 genes that exhibited increased expression in the MASH group compared to the control group. (G) 3D liver spheroids were treated with TGF-β or its inhibitor (TGFBi) for a week. Gene expression levels were measured by qPCR and normalized against physiological levels of free fatty acids. Asterisks (*) denote p value < 0.05 for statistical significance from ordinary one-way ANOVA.

Supplementary Information

Supplemental figure 1: Metabolomic analysis in this MASLD cohort. (A) Principal component analysis (PCA) diagrams for glycerolipids (GL) and non-glycerolipids (nonGL) in each matrix. (B) Plasma lipids with good correlations with liver lipids (r > 0.5) are depicted. (C) Metabolites associated with the disease progression in each matrix (q value < 0.05 or q value < 0.1). Compound classes with at least 5 hits associated with any histological feature were shown in the plot. (D) Commonly changed metabolites associated with steatosis across the three biological matrices. Significance values were calculated by –log10(p value)*sign(coefficient) from the linear regression models. (E) Chord diagram illustrating the edges that connect the metabolome in the three matrices as well as patients' metadata in the partial correlation network.

Supplemental figure 2: Heatmaps for pairwise analysis between lipid classes and clinical variables. Lipid classes analyzed in the liver (A), plasma (B), and conditioned medium (CM) (C) associated with clinical parameters. Linear regression analysis was performed for numerical variables, while one-way ANOVA was conducted for categorical variables. Significance values refer to –log10(p value) from linear regression models or one-way ANOVA.

Supplemental figure 3: Integrative map of the one carbon metabolism pathway. Pathway integration of metabolomic and transcriptomic data in the liver. Boxes were colored by significance values of associations between genes and steatosis (left) or fibrosis (right). Significance values refer to –log10(p value)*sign(coefficient) from linear regression models.

Supplemental figure 4: Unsupervised clustering of the liver transcriptome. (A) Principal component analysis (PCA) diagrams for gene expression, colored by

histological phenotypes and diagnosis (top right). (B) Associations between clinical metadata and principal components (PC1 - PC8) of the liver transcriptome.

Supplemental figure 5: Liver fibrosis and TGFβ-SMAD signaling target genes. (A) Selected genes involved in fibrosis-related signaling pathways. Boxes were colored by log2 fold changes of fibrosis grade 1, 2, and 3 (with the presence of steatosis) compared to fibrosis-free steatosis. (B) Heatmap of GTPase-related genes display a better correlation with fibrosis grades. Asterisks in the main heatmap denote the significance (p value < 0.05) from comparisons of each subgroup. Upregulated expressions of gene targets from TGFβ-SMAD signaling were observed in (C) and (D). Association with steatosis (S), NAS (N) and fibrosis (F) was indicated by black dots (q value < 0.05, left). Results were cross-referenced with two published cohorts (VA cohort, GSE130970; EU cohort, GSE135251) (*q value < 0.05 and with consistent direction of changes as in our cohort, bottom).

Supplemental figure 6: Partial correlation between genes in TGF-β signaling and other genes involved in tissue fibrosis-related signaling pathways. The subnetwork was extracted from the partial correlation network estimated from the transcriptome and metadata. Node size was determined by the significance value [–log10(p value)*sign(coefficient)] in the linear regression model for liver fibrosis.

Supplemental figure 7: Correlation matrix of gene expression levels between TGF-β and GTPase-related gene. The correlation plot was created of Pearson's r values for GTPase-related genes and TGF-β genes (*TGFB1* and *TGFB3*). The left annotation bar indicates the significance of associations between gene expression and fibrosis grades.

Supplemental figure 8: GTPase inhibition in LX-2 cells. (A) Workflow of the LX-2 experiment. TGFβ administration increased pro-collagen secretion by 32% (B) and collagen gene expression (C) in LX-2 cells. Pro-collagen secretion was determined by

ELISA and gene expression levels were assessed by qPCR. Asterisks "*" denote p value < 0.05 for statistical significance from unpaired t-test.

Supplemental figure 9: Illustration of GTPase regulation in the liver. TGF-β production is initiated in non-parenchymal liver cells, leading to the overexpression of GTPase regulators in both hepatic stellate cells and hepatocytes. This activation of GTPase signaling amplifies downstream fibrogenic effects, creating a feed-forward loop that intensifies fibrosis progression.

Supplemental figure 10: Autophagy regulation in the liver. Heatmap of autophagy genes in relation to histological features, indicating active lipophagy in the liver of obese individuals. Asterisks in the main heatmap denote the significance (p value < 0.05) from comparisons of each subgroup. Association with steatosis (S), NAS (N) and fibrosis (F) was indicated by black dots (q value < 0.05, left). Results were cross-referenced with two published cohorts (VA cohort, GSE130970; EU cohort, GSE135251) (*q value < 0.05 and with consistent direction of changes as in our cohort, bottom).

Supplemental Table 1: Gene overrepresentation analysis for genes associated with liver histological features.

References

1. Miao L, et al. Current status and future trends of the global burden of MASLD. *Trends Endocrinol Metab.* 2024;35(8):697-707.
2. Polyzos SA, et al. Obesity and nonalcoholic fatty liver disease: From pathophysiology to therapeutics. *Metabolism.* 2019;92:82-97.
3. Targher G, et al. MASLD: a systemic metabolic disorder with cardiovascular and malignant complications. *Gut.* 2024;73(4):691-702.
4. Yki-Jarvinen H. Non-alcoholic fatty liver disease as a cause and a consequence of metabolic syndrome. *Lancet Diabetes Endocrinol.* 2014;2(11):901-910.
5. Rodriguez LA, et al. Hepatocellular carcinoma in metabolic dysfunction-associated steatotic liver disease. *JAMA Netw Open.* 2024;7(7):e2421019.
6. Feng G, et al. Recompensation in cirrhosis: unravelling the evolving natural history of nonalcoholic fatty liver disease. *Nat Rev Gastroenterol Hepatol.* 2024;21(1):46-56.
7. Eslam M, et al. A new definition for metabolic dysfunction-associated fatty liver disease: An international expert consensus statement. *J Hepatol.* 2020;73(1):202-209.
8. Scoditti E, et al. Hepatic glucose metabolism in the steatotic liver. *Nat Rev Gastroenterol Hepatol.* 2024;21(5):319-334.
9. Piccinin E, et al. Metabolic aspects in NAFLD, NASH and hepatocellular carcinoma: the role of PGC1 coactivators. *Nat Rev Gastroenterol Hepatol.* 2019;16(3):160-174.
10. Fromenty B, Roden M. Mitochondrial alterations in fatty liver diseases. *J Hepatol.* 2023;78(2):415-429.
11. Bril F, et al. Metabolic and histological implications of intrahepatic triglyceride content in nonalcoholic fatty liver disease. *Hepatology.* 2017;65(4):1132-1144.
12. Younossi Z, et al. Global burden of NAFLD and NASH: trends, predictions, risk factors and prevention. *Nat Rev Gastroenterol Hepatol.* 2018;15(1):11-20.
13. Vvedenskaya O, et al. Nonalcoholic fatty liver disease stratification by liver lipidomics. *J Lipid Res.* 2021;62:100104.
14. McGlinchey AJ, et al. Metabolic signatures across the full spectrum of non-alcoholic fatty liver disease. *JHEP Rep.* 2022;4(5):100477.
15. Angulo P, et al. Liver fibrosis, but no other histologic features, is associated with long-term outcomes of patients with nonalcoholic fatty liver disease. *Gastroenterology.* 2015;149(2):389-97 e10.
16. Bataller R, Brenner DA. Liver fibrosis. *J Clin Invest.* 2005;115(2):209-218.
17. Subramanian P, et al. Fibrogenic pathways in metabolic dysfunction associated fatty liver disease (MAFLD). *Int J Mol Sci.* 2022;23(13):6996.
18. Powell EE, et al. Non-alcoholic fatty liver disease. *Lancet.* 2021;397(10290):2212-2224.
19. European Association for the Study of the Liver, et al. EASL-EASD-EASO clinical practice guidelines on the management of metabolic dysfunction-associated steatotic liver disease (MASLD). *J Hepatol.* 2024;81(3):492-542.
20. Hoang SA, et al. Gene expression predicts histological severity and reveals distinct molecular profiles of nonalcoholic fatty liver disease. *Sci Rep.* 2019;9(1):12541.
21. Govaere O, et al. Transcriptomic profiling across the nonalcoholic fatty liver disease spectrum reveals gene signatures for steatohepatitis and fibrosis. *Sci Transl Med.* 2020; 12(572):eaba4448.

22. Albaugh VL, et al. Proline precursors and collagen synthesis: biochemical challenges of nutrient supplementation and wound healing. *J Nutr.* 2017;147(11):2011-2017.
23. Tuohetahuntila M, et al. Lysosome-mediated degradation of a distinct pool of lipid droplets during hepatic stellate cell activation. *J Biol Chem.* 2017;292(30):12436-12448.
24. Koanantakool P, et al. In: Amos S, and Fernando P-C eds. *Proceedings of the Twenty-First International Conference on Artificial Intelligence and Statistics*. Proceedings of Machine Learning Research: PMLR; 2018:1376-86.
25. Liao Y, et al. Amino acid is a major carbon source for hepatic lipogenesis. *Cell Metab.* 2024;36(11):2437-48 e8.
26. Fabregat I, et al. TGF-beta signalling and liver disease. *FEBS J.* 2016;283(12):2219-2232.
27. Mashek DG. Hepatic lipid droplets: A balancing act between energy storage and metabolic dysfunction in NAFLD. *Mol Metab.* 2021;50:101115.
28. Dos Santos LRB, Fleming I. Role of cytochrome P450-derived, polyunsaturated fatty acid mediators in diabetes and the metabolic syndrome. *Prostaglandins Other Lipid Mediat.* 2020;148:106407.
29. Hajeyah AA, et al. The biosynthesis of enzymatically oxidized lipids. *Front Endocrinol (Lausanne).* 2020;11:591819.
30. Rath S, et al. MitoCarta3.0: an updated mitochondrial proteome now with sub-organelle localization and pathway annotations. *Nucleic Acids Res.* 2021;49(D1):D1541-D7.
31. Kisseleva T, Brenner D. Molecular and cellular mechanisms of liver fibrosis and its regression. *Nat Rev Gastroenterol Hepatol.* 2021;18(3):151-166.
32. Massague J, Sheppard D. TGF-beta signaling in health and disease. *Cell.* 2023;186(19):4007-4037.
33. Li Y, et al. Transforming growth factor beta latency: A mechanism of cytokine storage and signalling regulation in liver homeostasis and disease. *JHEP Rep.* 2022;4(2):100397.
34. Wen X, et al. LOXL2, a copper-dependent monoamine oxidase, activates lung fibroblasts through the TGF-beta/Smad pathway. *Int J Mol Med.* 2018;42(6):3530-3541.
35. Munger JS, et al. The integrin alpha v beta 6 binds and activates latent TGF beta 1: a mechanism for regulating pulmonary inflammation and fibrosis. *Cell.* 1999;96(3):319-328.
36. Huang H, et al. Rho-kinase/AMPK axis regulates hepatic lipogenesis during overnutrition. *J Clin Invest.* 2018;128(12):5335-5350.
37. Schwerbel K, et al. Immunity-related GTPase induces lipophagy to prevent excess hepatic lipid accumulation. *J Hepatol.* 2020;73(4):771-782.
38. Peng Y, et al. GP73 is a TBC-domain Rab GTPase-activating protein contributing to the pathogenesis of non-alcoholic fatty liver disease without obesity. *Nat Commun.* 2021;12(1):7004.
39. Agarwal H, et al. Rap1 Activation protects against fatty liver and non-alcoholic steatohepatitis development. *bioRxiv.* 2023.
40. Go CD, et al. A proximity-dependent biotinylation map of a human cell. *Nature.* 2021;595(7865):120-124.
41. Razick S, et al. iRefIndex: a consolidated protein interaction database with provenance. *BMC Bioinformatics.* 2008;9:405.
42. Huttlin EL, et al. Architecture of the human interactome defines protein communities and disease networks. *Nature.* 2017;545(7655):505-509.

43. Kardassis D, et al. Control of transforming growth factor beta signal transduction by small GTPases. *FEBS J.* 2009;276(11):2947-2965.
44. Panopoulou E, et al. Early endosomal regulation of Smad-dependent signaling in endothelial cells. *J Biol Chem.* 2002;277(20):18046-18052.
45. Wen Y, et al. Hepatic macrophages in liver homeostasis and diseases-diversity, plasticity and therapeutic opportunities. *Cell Mol Immunol.* 2021;18(1):45-56.
46. Dewidar B, et al. TGF-beta in hepatic stellate cell activation and liver fibrogenesis-updated 2019. *Cells.* 2019; 8(11):1419.
47. De Smet V, et al. Initiation of hepatic stellate cell activation extends into chronic liver disease. *Cell Death Dis.* 2021;12(12):1110.
48. Bell CC, et al. Characterization of primary human hepatocyte spheroids as a model system for drug-induced liver injury, liver function and disease. *Sci Rep.* 2016;6:25187.
49. Vorrink SU, et al. Endogenous and xenobiotic metabolic stability of primary human hepatocytes in long-term 3D spheroid cultures revealed by a combination of targeted and untargeted metabolomics. *FASEB J.* 2017;31(6):2696-2708.
50. Kemas AM, et al. Insulin-dependent glucose consumption dynamics in 3D primary human liver cultures measured by a sensitive and specific glucose sensor with nanoliter input volume. *FASEB J.* 2021;35(3):e21305.
51. Youhanna S, et al. Chemogenomic screening in a patient-derived 3D model of metabolic dysfunction associated steatohepatitis reveals the CHRM1-TRPM8 axis as a novel module for targeted intervention. *Adv Sci.* In press
52. Ratziu V, et al. Elafibranor, an agonist of the peroxisome proliferator-activated receptor-alpha and -delta, induces resolution of nonalcoholic steatohepatitis without fibrosis worsening. *Gastroenterology.* 2016;150(5):1147-59 e5.
53. Liu J, et al. Profiling the genome and proteome of metabolic dysfunction-associated steatotic liver disease identifies potential therapeutic targets. *medRxiv.* 2023.
54. Radosavljevic T, et al. Altered mitochondrial function in MASLD: key features and promising therapeutic approaches. *Antioxidants (Basel).* 2024; 13(8):906.
55. Saliba-Gustafsson P, et al. A functional genomic framework to elucidate novel causal metabolic dysfunction-associated fatty liver disease genes. *Hepatology.* 2024; in press.
56. Babiy B, et al. Dihydrosphingolipids are associated with steatosis and increased fibrosis damage in non-alcoholic fatty liver disease. *Biochim Biophys Acta Mol Cell Biol Lipids.* 2023;1868(7):159318.
57. Ooi GJ, et al. Hepatic lipidomic remodeling in severe obesity manifests with steatosis and does not evolve with non-alcoholic steatohepatitis. *J Hepatol.* 2021;75(3):524-535.
58. Wei W, et al. PTER is a N-acetyltaurine hydrolase that regulates feeding and obesity. *Nature.* 2024;633(8028):182-188.
59. Al-Baiaty FDR, et al. Possible hepatoprotective effect of tocotrienol-rich fraction vitamin E in non-alcoholic fatty liver disease in obese children and adolescents. *Front Pediatr.* 2021;9:667247.
60. Leszczynska A, et al. Extracellular vesicles as therapeutic and diagnostic tools for chronic liver diseases. *Biomedicines.* 2023; 11(10):2808.
61. Scorletti E, Carr RM. A new perspective on NAFLD: Focusing on lipid droplets. *J Hepatol.* 2022;76(4):934-945.
62. Van Woerkom A, et al. Hepatic lipid droplet-associated proteome changes distinguish dietary-induced fatty liver from glucose tolerance in male mice. *Am J Physiol Endocrinol Metab.* 2024;326(6):E842-E855.

63. Carr RM, et al. Reduction of TIP47 improves hepatic steatosis and glucose homeostasis in mice. *Am J Physiol Regul Integr Comp Physiol.* 2012;302(8):R996-1003.
64. Adeva-Andany MM, et al. Mitochondrial beta-oxidation of saturated fatty acids in humans. *Mitochondrion.* 2019;46:73-90.
65. Koliaki C, et al. Adaptation of hepatic mitochondrial function in humans with non-alcoholic fatty liver is lost in steatohepatitis. *Cell Metab.* 2015;21(5):739-746.
66. Bourne HR, et al. The GTPase superfamily: a conserved switch for diverse cell functions. *Nature.* 1990;348(6297):125-132.
67. Li Q, et al. Depletion of Rab32 decreases intracellular lipid accumulation and induces lipolysis through enhancing ATGL expression in hepatocytes. *Biochem Biophys Res Commun.* 2016;471(4):492-496.
68. Zou Y, et al. Rac2 deficiency attenuates CCl_4-induced liver injury through suppressing inflammation and oxidative stress. *Biomed Pharmacother.* 2017;94:140-149.
69. Ge J, et al. RhoA, Rac1, and Cdc42 differentially regulate alphaSMA and collagen I expression in mesenchymal stem cells. *J Biol Chem.* 2018;293(24):9358-9369.
70. Strickler JH, et al. Sotorasib in KRAS p.G12C-mutated advanced pancreatic cancer. *N Engl J Med.* 2023;388(1):33-43.
71. Morstein J, et al. Targeting Ras-, Rho-, and Rab-family GTPases via a conserved cryptic pocket. *Cell.* 2024;187(22):6379-92 e17.
72. Brunt EM, et al. Nonalcoholic fatty liver disease (NAFLD) activity score and the histopathologic diagnosis in NAFLD: distinct clinicopathologic meanings. *Hepatology.* 2011;53(3):810-820.
73. Kleiner DE, et al. Design and validation of a histological scoring system for nonalcoholic fatty liver disease. *Hepatology.* 2005;41(6):1313-1321.
74. Narayanaswamy P, et al. MetaboKit: a comprehensive data extraction tool for untargeted metabolomics. *Mol Omics.* 2020;16(5):436-447.
75. Gene Ontology C, et al. The Gene Ontology knowledgebase in 2023. *Genetics.* 2023; 224(1):iyad031.
76. Bindea G, et al. ClueGO: a Cytoscape plug-in to decipher functionally grouped gene ontology and pathway annotation networks. *Bioinformatics.* 2009;25(8):1091-1093.
77. Kanehisa M, et al. KEGG as a reference resource for gene and protein annotation. *Nucleic Acids Res.* 2016;44(D1):D457-462.
78. Otasek D, et al. Cytoscape automation: empowering workflow-based network analysis. *Genome Biol.* 2019;20(1):185.